

**DEVELOPMENT OF AIR DRYING METHODS  
FOR PAPERBOARD**

**TUNG JIAN SENG**

**UNIVERSITI TUNKU ABDUL RAHMAN**

# **DEVELOPMENT OF AIR DRYING METHODS FOR PAPERBOARD**

**TUNG JIAN SENG**


**A project report submitted in partial fulfilment of the  
requirements for the award of Bachelor of Engineering  
(Honours) Mechanical Engineering**

**Lee Kong Chian Faculty of Engineering and Science  
Universiti Tunku Abdul Rahman**

**May 2022**

## DECLARATION

I hereby declare that this project report is based on my original work except for citations and quotations which have been duly acknowledged. I also declare that it has not been previously and concurrently submitted for any other degree or award at UTAR or other institutions.

Signature :   
\_\_\_\_\_

Name : TUNG JIAN SENG  
\_\_\_\_\_

ID No. : 18UEB01654  
\_\_\_\_\_

Date : 16<sup>th</sup> May 2022  
\_\_\_\_\_

**APPROVAL FOR SUBMISSION**

I certify that this project report entitled “**DEVELOPMENT OF AIR DRYING METHODS FOR PAPERBOARD**” was prepared by **TUNG JIAN SENG** has met the required standard for submission in partial fulfilment of the requirements for the award of Bachelor of Engineering (Honours) Mechanical Engineering at Universiti Tunku Abdul Rahman.

Approved by,

Signature :



Supervisor :

DR. TING CHEN HUNT

Date :

16<sup>th</sup> May 2022

Signature :

Co-Supervisor :

Date :

The copyright of this report belongs to the author under the terms of the copyright Act 1987 as qualified by Intellectual Property Policy of Universiti Tunku Abdul Rahman. Due acknowledgement shall always be made of the use of any material contained in, or derived from, this report.

© 2022, TUNG JIAN SENG. All right reserved.

## **ACKNOWLEDGEMENTS**

I would like to thank everyone who had supported me to the successful completion of this project. Most of all, I would like to express my deep and sincere gratitude to my supervisor, Dr. Ting Chen Hunt. He has provided invaluable advices and showed an enormous patience in guiding me though out the project.

In addition, I would like express my gratitude to my loving parents and friends who had help me and given me encouragement in completing this project. Lastly, I would like to Universiti Tunku Abdul Rahman for the given chance to work on this project in completing my degree.

## ABSTRACT

Paperboard is a popular material that has been widely used as food packages, shirt boards and shoe midsole boards. In the current paperboard industry, an air drying method is adopted by drying the paperboard in an open-shed dryer. The solar energy has been widely applied in drying foods and crops. However, there is no review work was entirely contributed to the use of solar dryers in pulp and paper industry. Besides, drying paperboard in a high humidity and low temperature region through open-shed dryer could cause inefficient drying and the growth of microorganism such as fungus. The aim of this study is to develop an air-drying method which could improve the current drying process of paperboard. The study focused on the factors that affect the drying rate including the air flow, temperature and relative humidity (RH). Greenhouse solar dryer (GHSD) was introduced in this study to compare the drying performance with open-shed dryer. In this study, three-dimensional computational fluid dynamics (CFD) simulations were implemented to analyse the drying environment in the open-shed dryer and GHSD models with different openings configurations in a site having an ambient condition of 31 °C and 80% RH. From the results, it was found that the GHSDs have better drying performance than open-shed dryer with the controlled air flow, 6.7 to 32.6 °C higher temperature and 19.6 to 55.7 % lower RH. Besides, it was found that the drying environment in the GHSDs were strongly related to the openings configurations. A large opening area could results in high ventilation rate through the dryer which causes lower drying temperature due to the poor heat retention. Based on the results, an optimized design of GHSD was proposed with the idea of achieving a compromise between the ventilation and heat retention performance by implementing mechanical ventilation with natural ventilation. An exhaust fan was applied in the GHSD and the configuration of opening was modified. The proposed GHSD with optimized design has a better drying performance than the open-shed dryer by achieving 11.2 °C higher temperature and 29.8 % lower RH which led to an improvement of drying rate by 52.4 %. Also, it was recommended that the paperboard samples are oriented in parallel to the inflow of air during the drying process to ensure an uniform drying in the dryer.

## TABLE OF CONTENTS

<b>DECLARATION</b>		<b>i</b>
<b>APPROVAL FOR SUBMISSION</b>		<b>ii</b>
<b>ACKNOWLEDGEMENTS</b>		<b>iv</b>
<b>ABSTRACT</b>		<b>v</b>
<b>TABLE OF CONTENTS</b>		<b>vi</b>
<b>LIST OF TABLES</b>		<b>ix</b>
<b>LIST OF FIGURES</b>		<b>x</b>
<b>LIST OF SYMBOLS / ABBREVIATIONS</b>		<b>xii</b>
<b>LIST OF APPENDICES</b>		<b>xiv</b>
<b>CHAPTER</b>		
<b>1</b>	<b>INTRODUCTION</b>	<b>1</b>
1.1	General Introduction	1
1.2	Importance of the Study	2
1.3	Problem Statement	3
1.4	Aims and Objectives	4
1.5	Scope and Limitation of the Study	4
1.6	Contribution of the Study	4
1.7	Outline of the Report	5
<b>2</b>	<b>LITERATURE REVIEW</b>	<b>7</b>
2.1	Introduction	7
2.2	Drying Mechanism	7
2.2.1	Drying Curve	8
2.3	Factors Affecting Drying	9
2.3.1	Relative Humidity	11
2.4	Solar Drying	12
2.4.1	Open Sun Drying	13
2.4.2	Direct Solar Dryer	14



2.4.3	Indirect Solar Dryer	14
2.4.4	Mixed-mode Solar Dryer	15
2.4.5	Natural Convective Solar Dryer (passive)	15
2.4.6	Forced Convective Solar Dryer (active)	16
2.5	Greenhouse Solar Dryer	16
2.5.1	Geometrical Parameters	19
2.5.2	Cover Material	21
2.6	Application of Thermal Energy Storage System	22
2.6.1	Sensible Heat Storage System	22
2.6.2	Latent Heat Storage System	23
2.7	Computational Fluid Dynamics	24
2.7.1	CFD Analysis Procedures	24
2.7.2	Application of CFD in Greenhouse Solar Dryer	24
2.8	Summary	26
<b>3</b>	<b>METHODOLOGY AND WORK PLAN</b>	<b>28</b>
3.1	Introduction	28
3.2	Site and Description of the Dryers	29
3.3	Mathematical Model and Governing Equations	31
3.4	Radiation Model	32
3.5	Species transport model	33
3.6	Computational domain and mesh generation	33
3.7	Boundary conditions	37
3.8	Numerical method	41
<b>4</b>	<b>RESULTS AND DISCUSSION</b>	<b>43</b>
4.1	Introduction	43
4.2	Selection of planes and lines	43
4.3	Air flow distribution	44
4.4	Temperature distribution	48
4.5	Relative humidity	51
4.6	Thermal mass	54
4.7	Proposed design of dryer	55
4.8	Orientation of paperboard samples in the dryer	61
4.9	Summary	63

<b>5</b>	<b>CONCLUSION AND RECOMMENDATIONS</b>	<b>64</b>
	5.1 Conclusion	64
	5.2 Recommendations for future work	65
	<b>REFERENCES</b>	<b>67</b>
	<b>APPENDICES</b>	<b>75</b>

**LIST OF TABLES**

Table	Title	Page
Table 3.1:	Optical properties of materials	40
Table 3.2:	Physical properties of materials	40
Table 3.3:	Boundary conditions	41
Table 3.4:	The settings of CFD simulation	42

## LIST OF FIGURES

Figure	Title	Page
Figure 2.1:	Drying curve (Inyang et al., 2018)	8
Figure 2.2:	Influence of drying temperature on drying rate	10
Figure 2.3:	Open sun drying (Tomar, Tiwari and Norton, 2017)	13
Figure 2.4:	Schematic diagram of greenhouse drying (Tiwari, 2003)	17
Figure 2.5:	Passive mode glass-roof greenhouse solar dryer (Sharma, Chen and Vu Lan, 2009)	18
Figure 2.6:	Different shapes of greenhouse solar dryers (Vivekanandan et al., 2021)	20
Figure 3.1:	Flow chart for performing CFD simulations	28
Figure 3.2:	CAD models of (a) Open-shed and (b) GHSD	29
Figure 3.3:	Orientation of the dryer	29
Figure 3.4:	Opening configuration of G2 in (a) Isometric, (b) Front and (c) Back views	30
Figure 3.5:	Opening configuration of G3 in (a) Isometric, (b) Front and (c) Back views	30
Figure 3.6:	Computational domain for simulation	34
Figure 3.7:	Meshing of (a) Computational domain and (b) Dryer	35
Figure 3.8:	Cross sectional view of (a) Geometry and (b) Mesh of BOI	36
Figure 3.9:	Mesh metrics (a) Orthogonality, (b) Skewness and (c) Aspect ratio	37
Figure 3.10:	Logarithmic wind velocity profile	38
Figure 4.1:	Selected lines and planes of ((a) and (b)) Open-shed and ((c) and (d)) GHSDs	44
Figure 4.2:	Side view of velocity magnitude in (a) Open-shed dryer, (b) G1, (c) G2 and (d) G3	45

Figure 4.3:	Side view of velocity vector in (a) Open-shed dryer, (b) G1, (c) G2 and (d) G3	45
Figure 4.4:	Isometric view of air flow streamlines in (a) G2 and (b) G3	46
Figure 4.5:	Graph of air velocities along the height in Y	46
Figure 4.6:	Side view of temperature distribution in (a) Open-shed dryer, (b) G1, (c) G2 and (d) G3	49
Figure 4.7:	Graph of temperature along the height in Y	49
Figure 4.8:	Graph of temperature against mass flow rate	51
Figure 4.9:	Side view of RH distribution in (a) Open-shed dryer, (b) G1, (c) G2 and (d) G3	52
Figure 4.10:	Graph of RH along the height in Y	52
Figure 4.11:	Temperature distribution in soil and concrete floor after 1 hour and 30 minutes of cooling	55
Figure 4.12:	Opening configuration and location of exhaust fan on G4 in (a) Isometric, (b) Front and (c) Back views	56
Figure 4.13:	(a) Contour of velocity magnitude, (b) Velocity vector and (c) Air flow streamlines in G4	58
Figure 4.14:	Contours of (a) Temperature and (b) RH in G4	58
Figure 4.15:	Graphs of (a) Air velocity, (b) Temperature and (c) RH along the height in Y	59
Figure 4.16:	Orientations of paperboard samples in (a) Parallel and (b) Normal to inflow of air.	61
Figure 4.17:	Velocity vector around the paperboard samples oriented in (a) Parallel and (b) Normal to the inflow of air	62

## LIST OF SYMBOLS / ABBREVIATIONS

$a$	absorption coefficient
$C_1$	turbulent constant
$C_2$	turbulent constant
$C_\mu$	constant fitting parameter
$e$	actual vapor pressure ( $N/m^2$ )
$e_s$	saturation vapor pressure ( $N/m^2$ )
$E_i$	moisture source term
$H$	height (m)
$I$	radiation intensity ( $W/m^2$ )
$J$	water vapor diffusion flow
$k$	turbulent kinetic energy ( $m^2/s^2$ )
$K_0$	relative humidity range constant
$K_1$	relative humidity range constant
$L$	length (m)
$n$	refractive index
$N_i$	production rate of the water vapor
$P$	pressure (Pa)
$\vec{r}$	position vector
$s$	stroke length (m)
$\vec{s}$	direction vector
$\vec{s}'$	scattering direction vector
$t$	dry-bulb temperature ( $^{\circ}C$ )
$t_d$	dewpoint temperature ( $^{\circ}C$ )
$T$	temperature (K)
$u$	velocity (m/s)
$u_*$	friction velocity (m/s)
$u_i$	velocity component (m/s)
$u_j$	velocity component (m/s)
$W$	width (m)
$x_i$	coordinates (m)
$x_j$	coordinates (m)

$z$	height (m)
$z_0$	surface roughness coefficient length (m)
$\alpha_\lambda$	absorption coefficient
$\alpha$	absorptivity
$\varepsilon$	turbulent energy dissipation rate ( $m^2/s^2$ )
$\rho$	density, ( $kg/m^3$ )
$\mu_t$	turbulent dynamic viscosity ( $N \cdot s/m^2$ )
$\mu_l$	laminar dynamic viscosity ( $N \cdot s/m^2$ )
$\sigma$	Stefan-Boltzmann constant ( $5.669 \times 10^{-8} W/m^2 K^4$ )
$\sigma_l$	Laminar Prandtl number
$\sigma_s$	scattering coefficient
$\sigma_t$	turbulent Prandtl number
$\sigma_k$	turbulent constant
$\sigma_\varepsilon$	turbulent constant
$\Phi$	phase function
$\Omega'$	solid angle
$Y_i$	local mass fraction of water vapor
$\kappa$	von Karman's constant (0.42)
ABL	atmospheric boundary layer
BOI	boundary of influence
CFD	computational fluid dynamics
DSD	direct solar dryer
DO	discrete ordinates
GHSD	greenhouse solar dryer
ISD	indirect solar dryer
OSD	open sun drying
PCM	phase change material
RH	relative humidity (%)
SHSM	sensible heat storage material
UDF	user-defined function

**LIST OF APPENDICES**

Appendix	Title	Page
Appendix A:	UDF coding	75
Appendix B:	Contours of air temperature	76
Appendix C:	Contours of RH	78
Appendix D:	Contours and vectors of air velocity	80
Appendix E:	Graphs of temperature and RH along length in Z	83



## CHAPTER 1

### INTRODUCTION

#### 1.1 General Introduction

Paperboard is a popular paper-based material that is available in different grades based on the type of wood fibre used and the fabrication process. The paperboard products are widely used due to its advantages such as abundant availability, recyclability, flexibility, renewability, good biodegradability and ease of functionalization (Ham, Youn and Lee, 2020). The products consist of boards for food packaging, shirt board, and shoe midsole board. The global production of paperboard and paper is approximately 390 million tonnes, and it is predicted to reach 490 million tonnes by 2020 (Pratima, 2014). The growth of paper and paperboard industry is rapid in Asia. In this recent year, China and India are expected to become the key countries in the industry's growth.

The fabrication of paperboard is same as paper where they are made by removing water from wood fibres after wetting. Thus, the fabrication of paperboard requires similar major processes to paper fabrication. The major processes are pulping, optional bleaching, refining, sheet forming, pressing, drying, calendaring and winding (Selke, 2016). In the forming process, the diluted wood pulp fibres and water sludge form paper web through the combination of gravity drainage and application of suction below the forming fabric. The wet paper web is consolidated in the pressing process by removing the additional water with the mechanical pressure applied through the rotating rolls or a series of presses (Ghosh, 2011). According to a full set process for paperboard making provided by SHENZHEN HENGRENXING TECHNOLOGY CO.,LTD (2021), a company which is professional in manufacturing fourdrinier paperboard machine, the wet pressed paperboard will be moved to an open-shed dryer for air drying before proceeding to the hot press section.

Air drying is one of the common drying methods as of today. Forest Products Laboratory (1999) stated that air drying provides the least capital cost in removing water from wood during the early stages of drying. Same goes to application of air-drying method in paperboard making as paperboard is a wood

product. The water removal through air drying relies on the evaporation of the water content into dry air. It is a complicated heat and mass transfer process which requires heat supply, transfer of moisture within the object to its surface and then into the drying medium. The efficiency of air drying can be measured in term of drying rate. The increment of drying rate decreases the drying time needed. LV and Chen (2010) stated that it can be noticed that the drying process is important for production efficiency, cost and qualification. Most of the functional properties of paperboard are developed in the drying section (Ghosh, 2011). Therefore, it can be concluded that how to improve the drying rate is essential in developing air-drying method.

In this decade, solar energy is widely used as a sustainable and clean energy due to the increasing need of renewable energy because of limited fossil energy in the earth (Khanlari et al., 2020). Solar energy can be used in drying moist objects with the thermal heating from the sun. Solar drying such as open sun drying (OSD) has been adopted as a traditional method in drying crops, and other agricultural products since ancient times. In (2021) study, Abhay Lingayat et al. reported that there are many experimental, numerical and theoretical studies have shown the advantages of solar drying in agricultural and non-agricultural industries. There are three types of solar dryers which are active, passive and hybrid solar dryers. Greenhouse dryer is a new approach developed dryer to solve the drawbacks in OSD such as dust and rain. A greenhouse solar dryer (GHSD) is constructed in a greenhouse structure with insulation materials such as transparent glass, polyethene or polycarbonate. It traps the heat in an enclosure for a better drying and remove the moist with natural convection or forced air flow (Condorí and Saravia, 1998).

## **1.2 Importance of the Study**

Drying process is critical in paperboard making process as it has a great influence in the properties of paperboard. Natural air drying is the most preferred drying method due to its affordability. However, solar dyers such as GHSD can be applied in industrial and domestic drying process. According to Mondal et al. (2019), the efficiency of drying process can be affected by air temperature, humidity and air flow in the dryers. The air humidity depends on the air temperature. A GHSD heats up the air inside by receiving solar radiation

through insulation materials. Hot air can hold more moisture than cold air. Hence, heated air reduces the drying time of the product by enhancing the evaporation of moisture content with the lower relative humidity (RH) (Mohammad and Perera, 2007).

The increment of evaporated moisture content in the surrounding of paperboard increases the RH of the surrounding air. Increment in the humidity of the surrounding air reduces its capacity for carrying additional water vapor. This can hold back the evaporation rate of water content without a sufficient air flow around the paperboard. The high concentration of moisture around the paperboard may cause reabsorption of moisture into paperboard. This could result in a decreasing on drying rate. In GHSD case, although the heated air could enhance the drying rate, the slowdown of drying rate would still occur without an efficient air flow design within the desired space. Therefore, it is important to investigate the optimum parameters of air temperature, humidity and air flow to develop an efficient air-drying method.

### **1.3 Problem Statement**

There are many research and studies have been conducted on drying process of foods and crops with the application of solar thermal energy. However, despite they have shown the significant potential of the application of solar energy, there are only a few works focusing on bringing the solar thermal energy into industrial drying applications. Besides, there is no review work and study was entirely contributed to the use of solar dryers in various industries including pulp and paper industry.

Open shed drying is the current adopted air-drying method in paperboard industry. However, drying paperboard through open shed drying in high humidity and low temperature regions may result in inefficient drying process with longer drying time. Besides, the high humidity drying environment within the shed dryer may increase the risk of microorganism growth such as fungus. These difficulties can be overcome by applying GHSDs as the heated air reduces relative humidity and the UV radiation prevents the growth of fungus. Therefore, there is a need to investigate the performance of open shed drying and greenhouse solar drying to modify and improve the efficiency of current air-drying method.

#### **1.4 Aims and Objectives**

Based on the problems stated previously, the aim of this study is to develop an air-drying method which could improve the current drying process of paperboard. To achieve this aim, the objectives of this study are:

- (i) To investigate and compare the drying performance of open-shed dryer and different designs of GHSDs.
- (ii) To study the conditions within the dryers by implementing computational fluid dynamics (CFD) software.
- (iii) To optimize the parameters to achieve the best air-drying performance through modification of the dryer design.
- (iv) To study the effect of the orientation of paperboard samples on the drying process.

#### **1.5 Scope and Limitation of the Study**

The scopes and limitations of this study are listed as below.

- (i) The factors that have significant influence on the air-drying process will be determined and investigated in this study.
- (ii) The applications and reviews of various solar dryers will be investigated in this study.
- (iii) The performance of open-shed dryer and GHSD will be evaluated through CFD simulations.
- (iv) The improvised designs of dryer that can increase the drying efficiency and overcome the issues will be investigated.
- (v) The structural integrity of the dryer will not be considered in this study.
- (vi) The results of this study are not considering the change of weather condition around the dryer.
- (vii) The experimental work on investigating the drying rate of paperboard samples is not covered due to the pandemic which caused inaccessible to lab.

#### **1.6 Contribution of the Study**

In this study, the factors that greatly affecting the drying rate of paperboard drying through natural convection drying will be determined. The present work will be focused on developing air drying on paperboard with improved drying

performance and efficiency of the dryer. The drying time can be reduced with increment in drying rate and drying capacity. Besides, the reduced drying time could speed up the paperboard production process. The results of this study would provide guidelines for improving air drying process to paperboard industry.

Furthermore, this study involves development of an alternative air-drying method with the utilization of solar energy. Different types of solar dryers have been adopted in various industries. GHSD is an environmentally friendly air heater. Therefore, the performance of a GHSD will be investigated to explore the potential and applicability of GHSD in drying wet paperboard. The outcome of this study contributes to paperboard industry in utilizing solar dryers to enhance current adopted air-drying process.

## **1.7 Outline of the Report**

This report consists of five chapters which describe the workflow done in this project from introduction to conclusions and recommendations. The outline of this report is given as follows:

Chapter 1 presents the general introduction, importance of study, problem statement, aims and objective, scope and limitation of study and contribution of study which are important to determine the direction of this project.

Chapter 2 covers a literature review which includes the fundamentals of drying mechanism, factors affecting drying, solar drying which includes different types and modes of solar dryers. The works that had been done on developing GHSDs with various design parameters are reviewed and included in this chapter. A general introduction on CFD and analysis procedures to perform a CFD simulation are presented. Lastly, the applications of CFD in modelling of GHSDs are reviewed and included as well.

Chapter 3 presents the methodology for this project. Description on the CFD simulation setup which includes the equations used for computation, setting of parameters in the software, models developed for simulations, mesh generations and case studies performed, is included in this chapter.

Chapter 4 complies and analyzes the results obtained from the CFD simulation. Discussions on the results are also presented in this chapter.

Chapter 5 summarizes and concludes the findings of this study. Some improvements that can be achieved and recommended in the future study are included in this chapter.

## CHAPTER 2

### LITERATURE REVIEW

#### 2.1 Introduction

Drying process is an important section in paperboard making as it affects the efficiency of the production and the quality of paperboard produced. In order to have a better understanding to start this project, the fundamental of drying is first studied in this chapter. The application of solar dryers in various industries are reviewed from the research papers to investigate more about the effects of solar dryers in drying process. This section also evaluates the various types and designs of solar dryers to understand the different approaches and downsides on their performance. The factors affecting the drying process are reviewed to assist in deciding the improvement on dryer design.

#### 2.2 Drying Mechanism

The mechanisms of drying are mainly depending on the transport phenomenon of heat and mass transport processes simultaneously outside and inside of the drying materials. Therefore, there are two resistances which are the heat transfer and mass transfer. In a drying process, it consists of constant-rate and falling-rate periods of drying. Inyang et al. (2018) stated that normally hygroscopic products such as paper products dry at constant rate and following falling rate periods. The drying stops when the moisture content in the material has achieve equilibrium level. During the constant rate period, there is no internal and external mass transfer occurs and the existence of thin film of free water is considered at the material surface (Mohammad and Perera, 2007). Hence, the external heat transfer is controlling the drying in this period. Throughout the falling rate period, the drying is depending on the internal mass transfer resistance as a result of internal conditions and different moisture concentration in the material (Inyang, Oboh and Etuk, 2018). The transition from constant to falling rate at a certain moisture content is known as the critical moisture content.

### 2.2.1 Drying Curve

Drying curve is the plot of drying rate against drying time or moisture contents.

There are three major drying stages that can be noticed in the drying curve are:

- (i) Transient early stage, in which the material is heating up.
- (ii) Constant-rate period, in which the moisture is relatively easy to be removed.
- (iii) Falling-rate period, in which the moisture is bound within the material.

The drying rate curve is illustrated in Figure 2.1. The moisture content at which the transition from the constant rate to falling rate period happens is known as critical moisture content. Inyang et al. (2018) stated that the surrounding air temperature is normally higher than the temperature of the material in the initial drying period. Therefore, the drying rate increases in the beginning due to the increase in temperature of the material. The constant rate drying starts when the free water surface of the material is being evaporated. The falling rate starts when the surface of the material has been dried. Generally, two falling rate periods occur for both nonhygroscopic and hygroscopic materials (Mohammad and Perera, 2007). Hence, the material will experience a second falling rate period as the drying continues. Drying stops when the equilibrium moisture is reached.

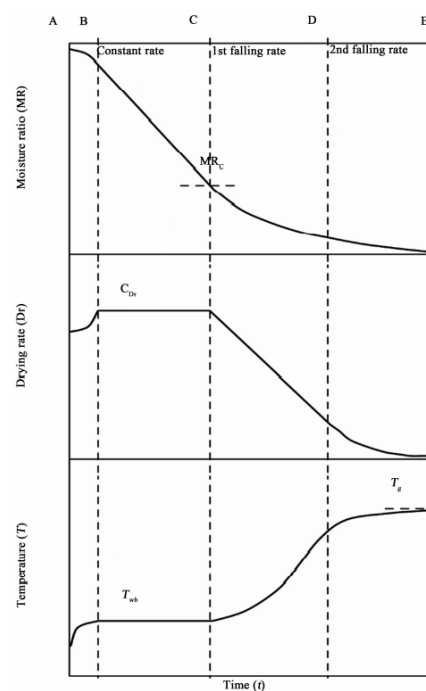


Figure 2.1: Drying curve (Inyang et al., 2018)



### 2.3 Factors Affecting Drying

Drying of both agricultural and non-agricultural products are significantly affected by various factors such as drying time, temperature of drying medium, relative air humidity, air velocity, surface area and thickness of the material (Chayjan, Alizade and Shadidi, 2012). Many researchers have studied the effects of air velocity, temperature and RH during drying process. In (2020) study, Chanpet et al. showed the drying time of the rubberwood decreased from 40 hours to 32 hours when the air velocity increased from 0.5 m/s to 3.5 m/s with a constant temperature and RH.

Caparanga et al. (2017) investigated the effects of air temperature and velocity on the drying process of arrowroot experimentally. The results showed the drying rate was increased by 69.3 % when the air temperature increased from 30 to 48 °C with constant air velocity. However, they found the increment in air velocity showed a little increment in the drying rate. In (2018) study, Xin et al. investigated the drying of tobacco strips at various air temperatures. It was reported that the drying time was reduced by 49.03 % with the increased air temperature from 60 to 80 °C. Chandramohan (2018) investigated influence of air flow velocity and temperature on drying parameters. The results showed that the drying time was reduced by approximately 45 % at 4 m/s and 46.5 % at 6 m/s while the drying temperature increased from 40 to 70 °C.

Doymaz (2005) studied the influence of drying temperature on the drying behavior of thin-layer mint leaves. The results showed that the drying time required to dry the mint leaves samples to a desired level at 55 °C was 420 mins shorter than 35 °C. Mabrouk and Mariem (2014) investigated the drying rate of tomato slices at different temperatures and air velocities. It was found that that drying time required was decreased by 38.6 % with the increased drying temperature from 38 to 57 °C at a constant air velocity. Besides, it was also found that the increased air velocity from 1 to 3 m/s with constant air temperature have shorten the drying time by 30 %.

Chandramohan (2018) investigated the effects of air temperature and velocity on drying a moist rectangular object. It was found that the drying rate has increased by 64.3 % when the air temperature increased from 40 to 70 °C. He also found the increment in air velocity from 4 to 6 m/s caused a little increment in drying rate. Hilphy et al. (2020) studied the effect of drying

temperature on drying tomato slices with constant air velocity. It was reported that the increment in air temperature from 60 to 80 °C showed an improvement of drying rate by 36 %.

Hashemi and Taghinezhad (2011) studied the influence of air drying temperature on drying rice. The result showed that the drying rate was able to increase by 4.5 times by increasing the air temperature from 40 to 60 °C. Ndukwu (2009) studied the influence of air temperature and velocity on the drying rate of cocoa bean. He found that it was able to improve the drying rate by 2 times with the increased temperature from 55 to 81°C. Besides, he also found that the drying rate was 50 % greater with the increased air velocity from 1.3 to 3.7 m/s. The influence of air temperature on drying rate is illustrated in Figure 2.2.

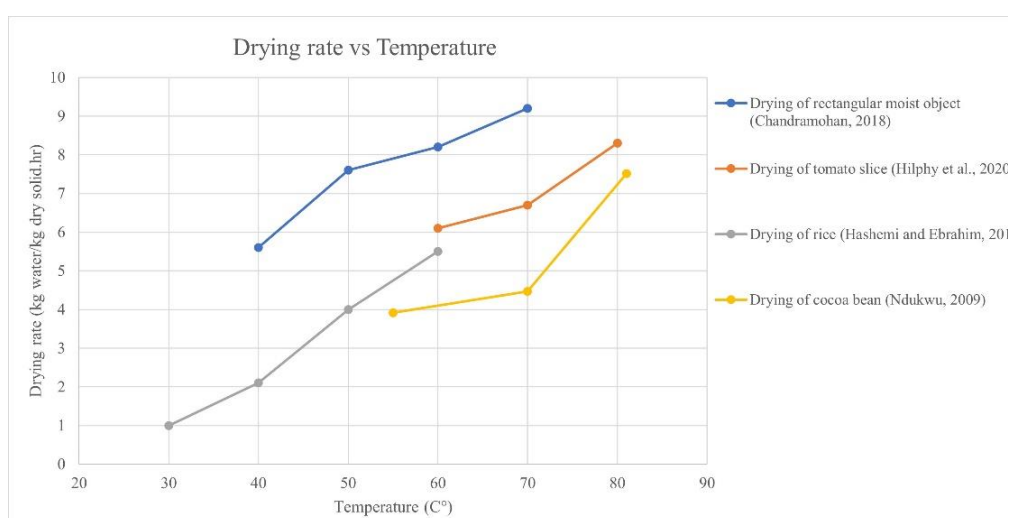


Figure 2.2: Influence of drying temperature on drying rate

There are experimental studies in the effect of air flow distribution in dryers on the drying rates have been performed by several researchers. It was concluded that the air flow distribution inside the dryers has a significant influence on the drying rate (Jamaledine and Ray, 2010). Mathioulakis et al. (1998) carried out the simulation of air flow distribution within an industrial tray air dryer with CFD approach. An uneven distribution of air flow within the dryer may cause nonuniform drying conditions (Jamaledine and Ray, 2010).

### 2.3.1 Relative Humidity

Relative humidity (RH) of air is explained as the ratio of the air vapor pressure to its saturation vapor pressure (Kong and Singh, 2011). It is a measure of the amount of moisture in the air compared to the amount of moisture required for the air to be fully saturated. In order to calculate RH (%), the equation is expressed as

$$RH = \frac{e}{e_s} \quad (2.1)$$

Where  $e$  is the actual vapor pressure ( $\text{N/m}^2$ ) and  $e_s$  is the saturation vapor pressure ( $\text{N/m}^2$ ) which means the maximum moisture amount the air that can hold at a provided temperature. The saturation vapor pressure increases with the increasing temperature (Curry, 2003).

Lawrence (2005) discussed several equations and proposed a modified equation to calculate RH with dry-bulb and dewpoint temperatures considering the accuracy and other approximations. Sargent (1980) proposed an equation that has the same basic form as Lawrence (2005) proposed but with a better accuracy:

$$t_d = t - K_0 + K_1 RH \quad (2.2)$$

Where  $t_d$  is the dewpoint temperature ( $^{\circ}\text{C}$ ),  $t$  is the dry-bulb temperature ( $^{\circ}\text{C}$ ),  $K_0 = 17.9$  and  $K_1 = 0.18$  for RH ranged from 65 to 100 %,  $K_0 = 22.5$  and  $K_1 = 0.25$  for RH ranged from 45 to 65 %. It indicates the RH decreases with increasing dry-bulb temperature.

Many researchers have investigated the effect of RH during drying process. The research by Ramirez et al. (2017) studied the effect of RH on drying apple slices. The experiment was carried out with three different RH which are 30, 50 and 70 %. The results showed that the drying rate was lower when the RH was increased from 30 to 70 % and the drying time has increased from 180 mins to 390 mins with a constant temperature of 50  $^{\circ}\text{C}$ .

Sasongko et al. (2020) studied the effect of RH on drying onion slices. The results showed that when the RH decreased from 40 to closely 10 %, the

drying time decreased from 173 mins to 129 mins at a constant temperature of 40 °C. Furthermore, Xu et al. (2021) investigated the effect of RH on drying finger citron slices. The result showed that the drying time was 35.4 % shorter when the RH decreased from 60 to 20 % at a constant temperature. Chanpet et al. (2020) investigated the influence of RH on drying rate of rubberwood. It was found that the drying rate was 66.7 % reduced when the RH increased from 6 to 67 % at a constant temperature. Therefore, it can be summarized that RH is highly dependent on the air temperature and drying time can be shorten with lower RH.

## **2.4 Solar Drying**

Solar drying is one of the utilizations of solar energy with the heat provided by the solar radiation of sun. Solar energy is understood as one of the cleanest energies that can be obtained from the universe to achieve humankind activity including drying (Tham et al., 2017). Thirugnanasambandam et al. (2010) reported that the total yearly solar radiation received by Earth is greater than 7500 times the global total annual consumed primary energy of 450 EJ.

Most of the countries are located in the climatic zones where they receive greater solar radiation incident than the mean solar radiation incident (Srinivasan and Muthukumar, 2021). The geographical locations of these developing countries make solar drying a good option for them. Therefore, solar drying can be used in various industries such as herbal products, textiles, pharmaceutical, fruit and food processing, wood and paper as it provides the advantages of low energy consumption, eco-friendly and able to be integrated with other heat sources (Bhaskara Rao and Murugan, 2021).

Solar dryers utilize additional systems and implements to harness radiative energy from the sun rays. In broad terms, solar dryers can be categorized based on their design of system, air circulation and solar contribution of the system. According to Mustayen et al. (2014), solar dryers can be categorized into six types including open sun drying, natural convection (passive mode), forced convection (active mode), direct, indirect and mixed mode solar dryers.

### 2.4.1 Open Sun Drying

Open sun drying (OSD) is the earliest drying method to dry agricultural and non-agricultural products since the ancient times (Lingayat, Balijepalli and Chandramohan, 2021). In the OSD, the products are directly exposed to the sun rays. The solar radiation falling on the product surface is not totally absorbed but partly reflected (Sahdev, Kumar and Dhingra, 2016). The absorbed solar radiation acts as heat source in heating up the surface. Hence, a part of the generated heat is used to remove the moisture content from the product surface to the surrounding air and then a part of this heat is lost to the ground and atmosphere (Sahdev, Kumar and Dhingra, 2016).

OSD has been the most selected drying method in tropical countries due to its affordability, especially in rural areas (Udomkun et al., 2020). However, the OSD has several drawbacks due to the risks of contamination by dust, rain, pests and animals which would cause quality degradation of the product. Besides, the parameters that would affect the drying rate such as solar radiation, air temperature, air velocity and RH are difficult to be maintained and controlled in OSD (Lingayat, Balijepalli and Chandramohan, 2021). Therefore, solar dryers are developed and continuous attempts were performed to enhance the designs of solar air drying methods and implements to overcome the drawbacks of OSD, such as the implementations of cabinet and greenhouse solar dryers (Srinivasan and Muthukumar, 2021).

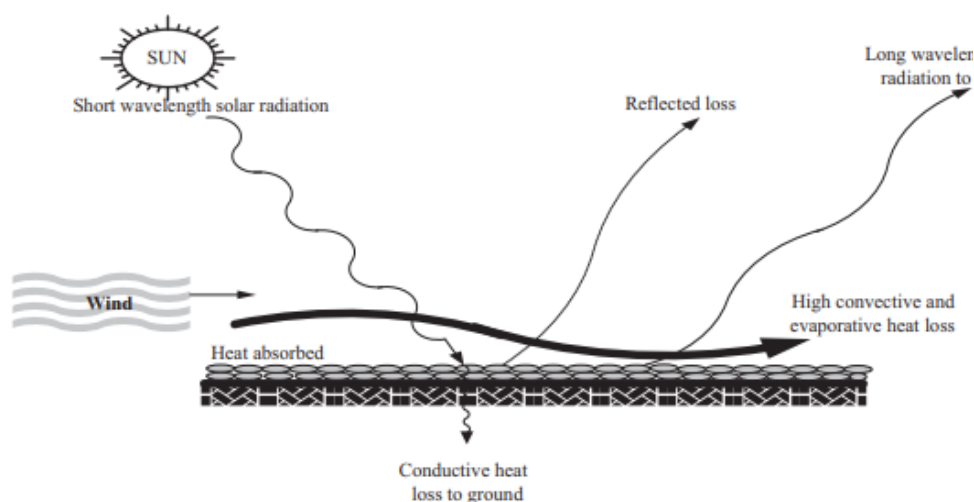


Figure 2.3: Open sun drying (Tomar, Tiwari and Norton, 2017)

### **2.4.2 Direct Solar Dryer**

The direct solar dryer (DSD) is one of the normally applied alternative ways of OSD method. It composed of a simple construction of drying chamber which has inlet, outlet and covered by transparent glazing for the transmission of solar radiation. The transparent glazing can be made up of different materials such as glass, plastic, polycarbonate, etc. (Lingayat, Balijepalli and Chandramohan, 2021). In this method, the product is placed in the drying chamber where they are directly exposed to the solar radiation. Heat is generated when the product has absorbed the solar radiation. The heat is then used to evaporates the moisture to dry the product (El Hage et al., 2018). The most widely used DSDs are cabinet and greenhouse solar dryers.

DSDs can be easily constructed as they are inexpensive, and a low maintenance cost is needed. Besides, the configuration of a direct solar dryer with the transparent cover simultaneously provides the product assured protection from rain and dust. An advanced method of using a DSD which is a cabinet dryer have been studied by Zomorodian and Dadashzadeh (2009). There are three parts in this this type of dryer which are the collector, air blower and drying cabinet. The drying cabinet has insulated walls and a glass cover. The glass cover reduced the direct convective temperature losses (Mustayen, Mekhilef and Saidur, 2014). However, Sharma, Chen and Vu Lan (2009) reported the main limitation of this kind of solar dryers is the drying product is directly expose to the solar radiation. This causes color and quality degradation of the products. Furthermore, the condensation of moisture formed inside glass cover during the drying reduces the transmittivity of the solar radiation (Sharma, Chen and Vu Lan, 2009).

### **2.4.3 Indirect Solar Dryer**

In the indirect solar dryers (ISD), the product is not directly exposed to the sun rays. An ISD is constructed of drying chamber which has an opaque cover and solar air collector (El Hage et al., 2018). The opaque cover prevents the product in the drying chamber from directly exposed to the sunlight. The solar air collector is linked to the drying chamber. The solar air collector receives solar radiation and heat up the atmospheric air within it. The heated air is then further driven into the drying regions by the fan (active type) or natural wind driving

force (passive type). In this type of solar dryer, the convective heat transfer between the heated air and product is responsible for the drying process (Lingayat, Balijepalli and Chandramohan, 2021). Many researchers reported ISD has higher thermal and drying performance. However, it has high capital cost and high maintenance is needed (El Hage et al., 2018).

#### **2.4.4 Mixed-mode Solar Dryer**

Mixed-mode solar dryer is a combination of the DSD and ISD (Kamarulzaman, Hasanuzzaman and Rahim, 2021). In mixed-mode solar dryer, a transparent cover is used to cover the drying chamber and it has a solar collector attached. The products in mixed-mode solar dryer are dried with direct exposure to solar radiation. Besides, the solar radiation is also received by the attached solar collector. Therefore, two sources of heat are provided to the drying chamber which are the direct exposure to solar radiation of the product and preheated air from the solar collector (Bhaskara Rao and Murugan, 2021). El Hage et al. (2018) reported that mixed-mode solar dryer has the greatest drying rate compared to DSD and ISD. A GHSD can be constructed in mixed-mode type. ELkhadraoui et al. (2015) investigated a new approach of mixed-mode type greenhouse experimentally.

#### **2.4.5 Natural Convective Solar Dryer (passive)**

As stated by Mustayen et al. (2014), a natural convective solar dryer requires minimum expenditure to control the drying temperature. In the natural convective solar dryer, the air within the drying chamber is heated up by incident solar radiation. The heated air has a lower density than the surrounding air. Therefore, the buoyancy effect is created because of the density variation between the heated air in the drying enclosure and the surrounding ambient air (Srinivasan and Muthukumar, 2021). The air will be driven out of the dryer by this phenomenon. Natural convective working principle can be applied in DSD and ISD.

This type of solar dryers usually plays an important role in the drying sector due to its low cost. Besides, it has been generally applied in drying agricultural products due to its simple operation and maintenance. According to Kumar, Sansaniwal and Khatak (2016), the drying efficiency of passive dryers

falls in the range of 20 to 40 % depending on the type of materials, rate of airflow and orientation. However, the passive solar drying system has a limited capacity. Furthermore, the drying rate is greatly influenced by the atmospheric conditions due to the little float to induce air flow within the dryer (Mustayen, Mekhilef and Saidur, 2014).

#### **2.4.6 Forced Convective Solar Dryer (active)**

In the forced convective solar dryer, there is a ventilation system which consist of fans or blowers to circulate the air within the drying chamber (Udomkun et al., 2020). The forced convective system can be applied in both DSD and ISD. In active mode ISD, a fan of blower is applied to transfer the heated air from the solar collector to drying chamber. Active solar dryers have higher drying efficiency than passive solar dryers (Patil and Gawande, 2016). Electricity is required to operate the fan and blower. Therefore, a greater investment is required for active dryers and it is more difficult to maintain and operate compared with passive dryers (Udomkun et al., 2020). However, several researchers have found that active solar dryers are better than passive solar dryers in terms of controlling the drying parameters (Tiwari, Tiwari and Al-Helal, 2016).

### **2.5 Greenhouse Solar Dryer**

Greenhouse solar dryer (GHSD) is a system that utilizes the standard greenhouse structure to operate as a solar dryer through warmer periods of the day in sunny areas. The GHSD is an enclosed framed structure with transparent walls and roofs made up of glass, polyethylene sheet, etc (Sahdev, Kumar and Dhingra, 2016). It is widely adopted in various industries such as agricultural and food, rubber, sewage and industrial waste (Lingayat, Balijepalli and Chandramohan, 2021). It is the advanced method of solar drying being used to overcome the limitations of open sun drying method such as contaminations due to dust, dirt, animals, etc. Basically, a GHSD operates either in passive or active mode. It is categorized as DSD primarily and it can be categorized as mixed-mode type when it combines with solar collector (ELkhadraoui et al., 2015; Srinivasan and Muthukumar, 2021). The working principle of a GHSD is shown in Figure 2.4. It traps short wavelength solar radiation and stores the long



wavelength thermal radiation to form a favorable micro-climate drying (Odhiambo, 2016). The dryer receives the solar radiation through the transparent cover to heat up the air and dry the product through natural or forced air circulation within the dryer.

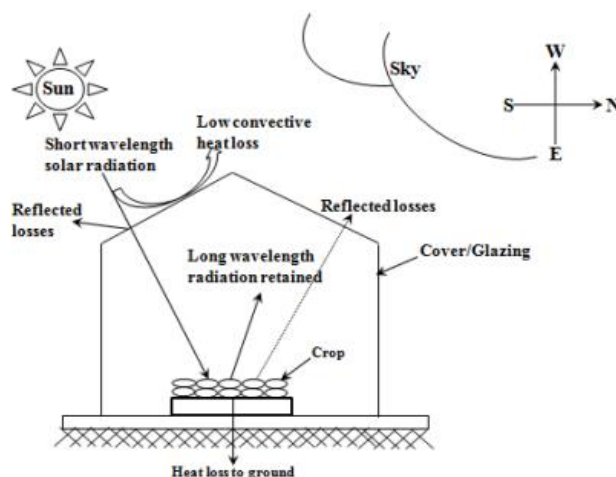


Figure 2.4: Schematic diagram of greenhouse drying (Tiwari, 2003)

Many experiments and research have been performed to investigate and improve the performance of GHSD. The Brace Research Institute glass-roof solar dryer was the earliest configuration of practical passive mode GHSD (Sharma, Chen and Vu Lan, 2009). The dryer (Figure 2.5) has a fixed slanted transparent glass roof and a ridge cap made of folded zinc over the roof as an air exist vent. Badaoui et al. (2019) developed an active mode GHSD to investigate the drying of tomato pomace waste. The dryer has four sides with a  $36^\circ$  inclines roof. The sides and roof of the dryer were covered with transparent polycarbonate sheets which has 70 % transmittance value and black polystyrene was used as insulation at the rear wall. The results showed that the products are able to be dried at temperature range of 40 to 58 °C within 5 hours in the dryer.

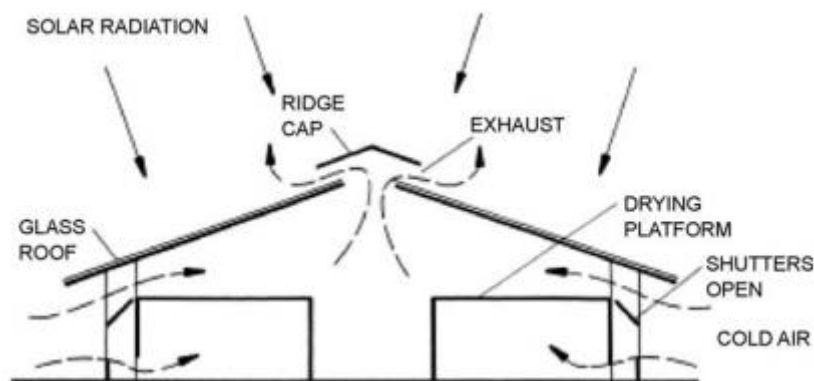


Figure 2.5: Passive mode glass-roof greenhouse solar dryer (Sharma, Chen and Vu Lan, 2009)

Ayyappan et al. (2016) studied the thermal performance of a natural ventilated GHSD with the integration of thermal storage materials such as concrete, rock bed and sand. The dryer was used to dry coconuts. The GHSD was constructed of UV stabilized polyethylene sheet with a thickness of 200 microns. The dryer was designed in a semi-circular shape standing over a black painted floor which is made of concrete. Turbo vent fan is installed to maintain the air flow within the dryer. The drying time with the use of rock bed as compared to sand and concrete floor was obtained. The result showed that the concrete floor has increased the temperature of day and nighttime by 16 °C and 3 °C respectively compared to the ambient temperature. The moisture content of coconuts decreased from 52 to 7 % (w.b.) within 78 hours. It was reported that the drying time had been reduced by 55 % as in open sun drying 174 hours were used to achieve the same moisture level. The average efficiency of the dryer was found to be 9.5 %.

Almuhanna (2012) investigated the feasibility of using a GHSD for drying dates. A gable-even span GHSD was designed and installed at King Faisal University, Saudi Arabia. The dimension of the dryer was 2 m (L) × 1 m (w) × 1.2 m (H) and constructed of 800 µm thick flat fiberglass sheet with transmittance value of 77.48 %. The roof was inclined at 30 °. An electrical axial fan was installed at the air outlet. It was able to provide airflow rate of 5.5 m<sup>3</sup>/min. The thermal performance analysis was carried out. The result showed that the air temperature within the dryer was 14.1 °C higher and the RH was

9.6 % lower compared to ambient air. It was also concluded that the overall thermal efficiency of the GHSD was 60.11 %.

Jitjack et al. (2016) developed a parabolic shaped GHSD in Rajamangala University of Technology Tawan-Ok in Chonburi, Thailand. The dryer was used to dry rubber sheets. The dryer was built with the dimension of 3.5 m (L)  $\times$  2 m (w)  $\times$  1.5 m (H) and it was modifiable to increase the area of the base which is 3.5 m (L)  $\times$  3 m (w). The dryer was covered by transparent polycarbonate sheets with transmittance value of 77 %. The base of the dryer was made of concrete with a black painted top surface to enhance the absorption of solar radiation. An electric fan was installed at the rear wall to exhaust the humid air. The result showed that the temperature within the dryer was in a range of 30 to 50 °C where the ambient temperature was around 30 °C. Besides, the dryer was able to provide maximum temperature of 55 °C with area-enhanced panels. It was reported that the dryer with area-enhanced panels has shorter drying time than without area-enhanced panels.

Jain and Tiwari (2004) developed a roof type even span GHSD that was constructed of PVC pipes and UV stabilized film sheet. The dryer was used to dry samples of cabbage and peas as thin layers under the climate conditions of New Delhi, India. An air vent was provided at the roof for natural air circulation and a fan was installed at the sidewall to provide air circulation with an air velocity of 5 m/s during the active mode of drying. The experiment determined the drying time by finding the convection heat transfer coefficient and using a developed empirical relation. The result reported that the air temperature within the dryer varied from 31 to 48 °C while the ambient temperature ranged from 30.4 to 39 °C. It was reported that the moisture removal rate was higher in active mode drying due to the decreasing of RH within the dryer.

### **2.5.1 Geometrical Parameters**

The geometric configurations such as shape and orientation are the main design parameters of a GHSD (Afou et al., 2015). These parameters decide the maximum solar radiation that can be collected by the dryer. In the study by Sethi (2009), the influences of different shapes (even, uneven, arch, Quonset and vinery) and orientations (north-south and east west) of GHSDs on the air

temperature within the dryer with similar dimensions was investigated. The results showed that the GHSD in uneven-span shape received greater solar radiation but the Quonset shaped GHSD received the lowest solar radiation where both of the dryers were located at east-west orientation. A similar result was reported by Dragičević (2011) that the GHSD in uneven-span shape located at east-west orientation received a higher solar radiation than north-south orientation.

Mobtaker et al. (2019) investigated the performance of GHSDs in different shapes (single, uneven, even, arch, Quonset and vinery), and orientations. The results showed that the GHSD in single span shape located at east-west orientation received higher solar radiation among the tested shapes. Gupta and Chandra (2002) studied the performance of GHSD in various shapes (gable, Quonset and gothic arch). The results showed that the gothic shaped GHSD located at east-west orientation has lower energy requirement to heat up the air compared to other shapes. However, Odhiambo (2016) adopted Quonset shape as it was found that Quonset shape provided a better structure to support the axial fan and other mounting structures with the least condensation of moisture on the walls. Furthermore, Vivekanandan et al. (Vivekanandan et al., 2021) carried out experimental and CFD study on different shapes. Quonset shape was suggested as the ideal shape. The different shapes of GHSD are illustrated in Figure 2.6.

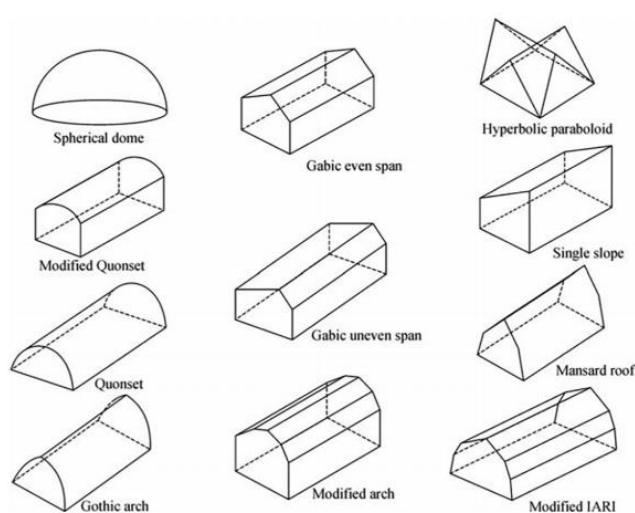


Figure 2.6: Different shapes of greenhouse solar dryers (Vivekanandan et al., 2021)

### **2.5.2 Cover Material**

The option of the GHSD cladding material is guided by the cost, durability, the necessity for high heat retention, long-term UV stability, light transmissivity and low vapor condensation (Lexan, 2015; Odhiambo, 2016). Plastics, glass, and thin-film sheets are generally used as the covering material. Lexan (2015) recommended the materials to cover a GHSD which are film plastic, rigid plastic and glass.

Polyethylene materials are the recommended plastic films due to its UV stabilization, infrared inhibition and low cost. Plastic films with infrared inhibitor are able to reduce the heat loss within the GHSD by up to 20 % during night time (Odhiambo, 2016). The UV stabilized films are usually available in various thickness from 150 to 1000 microns with lifespans of 3 to 4 years. Polyethylene films are commonly used with thickness of 400 microns (Lexan, 2015). Besides, the innovation of anti-condensate additive in film coverings prevents the moisture buildup from running down onto the drying products (Lexan, 2015). This new type of film also prevents the condensation from blocking the sun rays.

Fiberglass, acrylic and polycarbonate which are known as rigid plastics usually come in corrugated and flat forms. They are shatterproof materials. Odhiambo (2016) stated that rigid plastics are suggested for GHSDs intended to endure for over 10 years. All rigid plastics have great heat retention. Fiberglass is able to retain 4.4 and 70.8 times more heat efficiently than glass and polyethylene respectively. These materials cost five times higher than plastic films. However, they are more cost effective than the plastic films in the long term (Odhiambo, 2016). Lexan (2015) stated that the light transmissivity of fiberglass is similar to glass material. Acrylic materials have better light transmissivity than polycarbonate. However, plain fiberglass was found to get yellowish with time and restrains the light transmission.

Glass has been preferred as greenhouse covering traditionally for permanence. As stated by Odhiambo (2016), tempered glass is the ideal material for greenhouse covering. They have great resistance to impact and able to resist the expansion and contraction throughout the temperature changes. A single-pane glass with 3 mm thickness is sufficient for greenhouses. Greater strength and additional insulation value can be obtained by increasing the thickness to 4

mm (Odhiambo, 2016). Tempered glass has higher cost than polycarbonate but provides better durability and resistance to scratch. Besides, it is clear and provide no diffusion (Odhiambo, 2016). However, stronger structural elements are required to withstand the weight of glass and it is more difficult to be installed (Lexan, 2015).

## **2.6 Application of Thermal Energy Storage System**

The variation in solar radiation during the day causes the variation in the air temperature. To obtain continuous drying process within the GHSD has become an attempt to improve the performance of the dryer. It can be solved with the installation of a thermal storage system into the dryer. There are two kinds of thermal storage system including sensible heat and latent heat storage system. In sensible heat storage system, the thermal energy is stored by increasing the temperature of a solid or liquid (Agrawal and Sarviya, 2016). In latent heat storage system, latent heat is absorbed or released at a constant temperature when the material changes its phase from solid to liquid or liquid to gas (Agrawal and Sarviya, 2016).

### **2.6.1 Sensible Heat Storage System**

The total heat that can be stored and collected in a sensible heat storage material (SHSM) is determined by three parameters including the temperature difference, quantity and heat capacity of the material (Srinivasan and Muthukumar, 2021). The materials charging and discharging capacity changes depending on these parameters. The generally used SHSMs are concrete, gravel, rock, brick and sand. The SHSMs provide lower heat storage capacity than phase change materials. However, the main advantage of SHSMs is they are available at a lower cost.

In a GHSD, SHSMs are used as the base or covering to the floor in the dryer. In the study by Ahmad and Prakash (2020), they investigated the performance of various bed condition including black gravel, ground, concrete, and gravel beds in a passive mode GHSD. The result showed that the black gravel bed provided maximum heat gain of 53 % and temperature of 64 °C followed by gravel, concrete and ground bed respectively. In the study by Natarajan et al. (2017), it was reported that the sand bed was able to improve

the drying performance by providing a greater air temperature within the GHSD when compared to OSD and dryer without SHSM. Ayyappan et al. (2016) studied different SHSMs integrated with the GHSD. The results reported that rock bed with 4 inches thickness had reduced 121 hours of drying time when compared to OSD.

The thickness of the SHSM bed is important in retaining the temperature variation between the ambient conditions and dryer. Ayyappan et al. (2016) investigated different thickness of sand and rock bed throughout day and night time within the GHSD. The results showed that the performance of sand and rock bed with 4 inches thickness provided better drying performance than 5 inches thickness.

## **2.6.2 Latent Heat Storage System**

Phase change materials (PCM) are used in latent heat storage system to perform the thermal energy storing. PCMs are categorized into three types which are organic, inorganic and eutectic types. As stated by Agrawal and Sarviya (2016), the preferred thermo-physical properties of PCMs included low supercooling, high density, long term stability, small volume change during phase change, high thermal conductivity and high latent heat capacity. The cost effectiveness and availability of the material are important in selecting a PCM for the GHSD.

Azaizia et al. (2020) studied the performance of the GHSD with and without the use of thermal storage system. Paraffin wax was the selected PCM in the study. The result showed that the air temperature within the GHSD with PCM was 5 to 19 °C greater than the ambient air for around 11 hours. The dryer with PCM provided a shorter drying time of product with 25 and 45 hours lower than the dryer without PCM and OSD respectively. Berroug et al. (2011) investigated the performance of passive mode GHSD integrated with calcium chloride hexahydrate as PCM integrated on the north wall with various thickness of 2 to 5 cm. It was reported that 4 cm was the optimum thickness which provided an increment of air temperature (6 to 12 °C) within the dryer at night time. Boulard et al. (1990) investigated the performance of a GHSD with the use of paraffin as PCM. The results showed that the air temperature within the dryer was averagely 6.6 °C greater than the ambient air at night time.

## **2.7 Computational Fluid Dynamics**

Computational Fluid Dynamics (CFD) simulates a phenomena involving fluid-flow based on the conservation laws including the conservation of energy, momentum and mass in governing the fluid motion. It involves the modeling based on the principles of fluid dynamics and numerical methods in solving complex fluid flow problems.

### **2.7.1 CFD Analysis Procedures**

In order to obtain and solve the solution from CFD simulation, the procedures to be performed are presented as below. (Cengel and Cimbala, 2009)

1. The geometry or computational domain of model is created.
2. The geometry domain is discrete into a finite number of elements (meshing). The generated meshes could be uniform or non-uniform. However, the solution is greatly depending on the mesh quality. Hence, it is recommended to check the mesh quality before proceeding to the next step.
3. Solution algorithm and numerical parameters including the continuity equation, momentum equation, energy equation, turbulence models and pressure-velocity coupling are selected.
4. The boundary conditions of the domains are defined on the edges or faces.
5. The types (water, air, gasoline, etc.) and properties (temperature, viscosity, density, etc.) of the fluid domain are specified.
6. The iterative calculations of the equations are performed with initial conditions until a converged solution is obtained.
7. Lastly, the result is analyzed once the solution has converged.

### **2.7.2 Application of CFD in Greenhouse Solar Dryer**

CFD could provide an effective means of accurately computing the indoor climatic variables of ventilated structures under different design conditions inside a virtual environment (Norton et al., 2007). Due to the rapid development of computer technology, the CFD has been widely used in modelling GHSDs to study and predict the drying efficiency of products. The CFD simulations are applied to determine the air temperature, product temperature and air flow



distribution within the dryer. He et al. (2018) stated that CFD has been proved to be used as an effective simulation tool to study microclimate within GHSDs with low cost and reliable results. Many researchers have utilized CFD as a tool to evaluate the performance of GHSDs.

Román-Roldán et al. (2019) investigated the air temperature and velocity within the GHSD. The discrete ordinate (DO) method and  $k-\epsilon$  realizable model were applied in this study. The results showed the non-homogenous temperature distribution due to the higher turbulent kinetic energy in the middle of the drying section. It was reported that reduction of the dryer volume under similar operating conditions is important in achieving higher air velocity and drying efficiency. Li et al. (2020) investigated the air temperature and airflow pattern within an arched GHSD. The realizable  $k-\epsilon$  turbulence model and DO model were applied in the simulation. It was reported that the proposed design with an optimum angle at the opening has provided good air exchange capacity where the velocity and temperature inhomogeneities were approximately reduced by 11.89 % and 33.3 % respectively. Mellalou et al. (2021) studied the performance of a natural ventilated uneven-span GHSD at no-load condition. The  $k-\epsilon$  turbulence model and DO model were applied in the simulation. The air temperature within the dryer was found in the ranges of 36 to 50 °C and 30 to 56 °C in two different days. It was reported that the average air temperature within the dryer was 48.71 % and 45.70 % greater than the ambient air in day-1 and day-2 respectively.

Villagran et al. (2020) investigated the natural ventilation behavior in a flat roof greenhouse. The standard empirical  $k-\epsilon$  model and DO model were applied in this simulation. The results showed that the areas with higher temperatures within the dryer coincide with the areas with poor airflow and low air velocity. Besides, it was found that the high temperature areas within the dryer have low RH. Piscia et al. (2012) investigated the condensation of humid air within a four spans GHSD. The standard empirical  $k-\epsilon$  model and DO model were applied in this study. It was stated that DO model is recommended for semi-transparent materials. The roof and air temperature, condensation rate and RH were obtained. The results showed that the roof has the lower temperature and most of the condensation occurred at the roof. It was reported that it may be

possible to control the humidity and condensation within the dryer by controlling the roof temperature.

Validation studies have also been performed by the researchers to study the differences of the experimental results and CFD results. Li et al. (2020) verified the simulation results with experimental results by calculating PRMSD and NMSE of the air temperature within the dryer. The calculated PRMSD and NMSE were 5.69 % and 9.95 % respectively. Hence, it was reported that a good agreement between the simulation and experimental results were achieved. Mellalou et al. (2021) compared the simulation and experimental results of the air temperature within the dryer. An acceptable difference between the simulated and measured results were found not exceeding 8.46 °C. Boulard and Wang (2002) compared the simulation and experimental results of solar radiation, airflow and temperature distributions with plotted graphs. It was found good agreement between the simulated and experimental results.

Most of the studies have shown that CFD are broadly applied in predicting the air temperature, airflow distribution, air velocity, RH, etc. which are important in determining the performance of a GHSD with good agreement between simulated and experimental results. Therefore, it can be confirmed that CFD is an appropriate and flexible tool to study the performance of a GHSD with different boundary conditions.

## **2.8 Summary**

In this section, the fundamental of drying mechanism was studied to gain a better understanding to start this project. The air temperature, airflow distribution and RH are the critical factors affecting the drying efficiency of various dryers. It was found that higher air temperature, uniform airflow distribution and lower RH are recommended to improve the drying efficiency. GHSDs are possible to be implemented in active or passive modes to provide better drying efficiency. The selection of GHSD design is based on the shapes, orientations and materials. Among the various shapes reviewed, the even span and Quonset are the most adopted shapes in the designs. The east-west orientation was found to have better absorption of solar radiation into the dryer. Thermal storage system can be considered to improve the performance of the dryer. Furthermore, CFD simulation can be applied to predict the RH, air

temperature and airflow distribution within the dryer. Predicting these parameters helps in designing and developing the dryer. Most of the reviewed studies applied DO model, standard and realizable k- $\epsilon$  turbulence model in their simulations.

## CHAPTER 3

### METHODOLOGY AND WORK PLAN

#### 3.1 Introduction

The aim of this project is to develop and optimize the air-drying method by comparing the performance of open-shed dryer and GHSD. The important factors affecting the drying efficiency including the airflow, air temperature and RH within the dryers will be investigated using CFD software. The configurations of open-shed dryer and GHSD will be implemented to perform the investigations. Furthermore, the GHSD with different openings configurations will be tested through simulations. The results of the simulations will be analyzed to investigate the drying efficiency of the dryers. Lastly, a dryer with an optimized drying performance will be proposed based on the evaluated results. The flow of methodology for conducting the CFD simulation is presented as below:

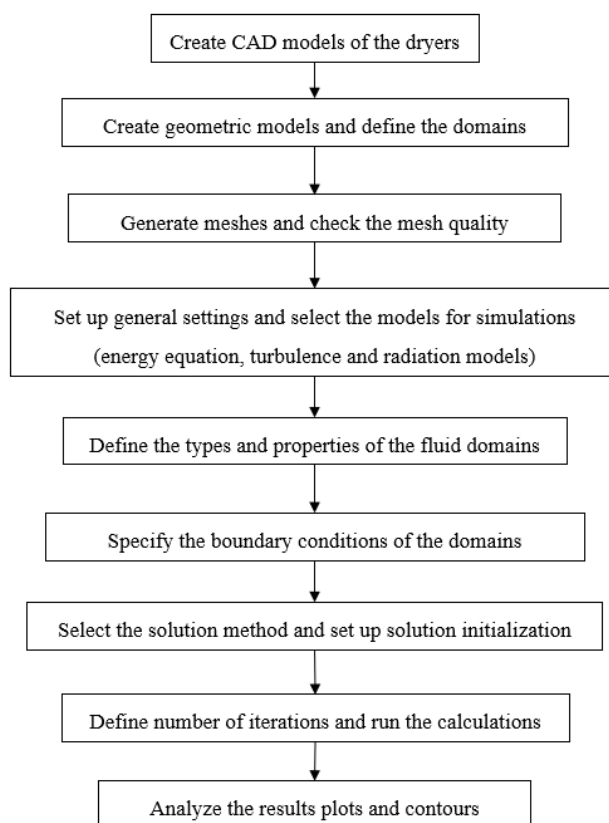


Figure 3.1: Flow chart for performing CFD simulations

### 3.2 Site and Description of the Dryers

The dryers were constructed at Universiti Tunku Abdul Rahman (UTAR), Kuala Lumpur, Malaysia (3.0394 °N, 101.7941 °E) in the time zone of GMT +8. The original dimensions of the dryers were considered in this project. The structures of the open-shed dryer and GHSD are shown in Figure 3.2. Both of the open-shed dryer and GHSDs have the similar dimensions which are 3.66 m (W) × 6.1 m (L) × 5.18 m (H). Concrete floors with thickness of 0.2 m were implemented in the open-shed dryer and GHSDs. Besides, the dryers were oriented in the east-west direction as this orientation is able to receive higher amount of solar radiation compared to north-south orientation (Figure 3.3) (Naamandadin, Sapian and Noor, 2016). The open-shed dryer has a gable roof which is made of zinc sheet. The thickness of the roof is 1 mm.

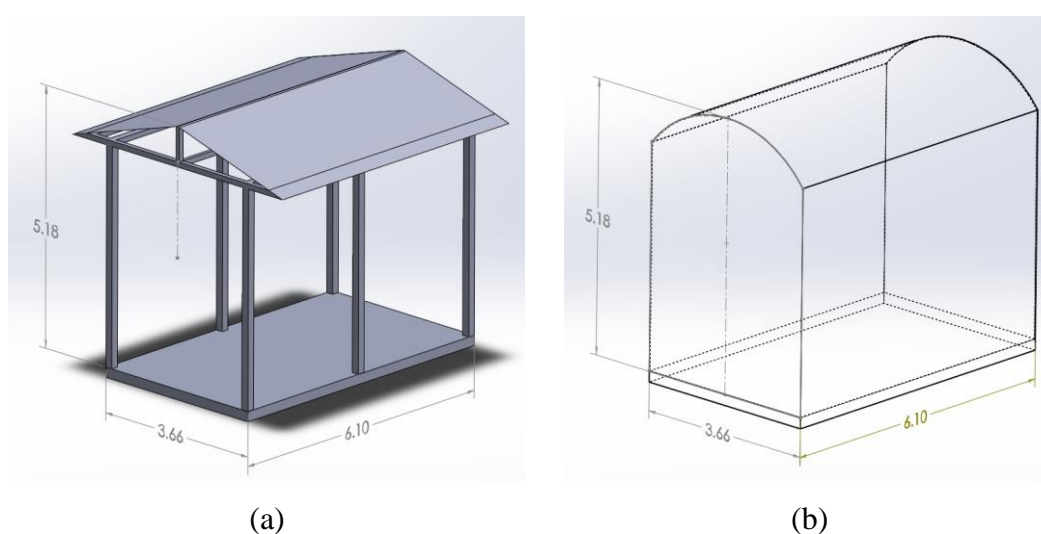


Figure 3.2: CAD models of (a) Open-shed and (b) GHSD

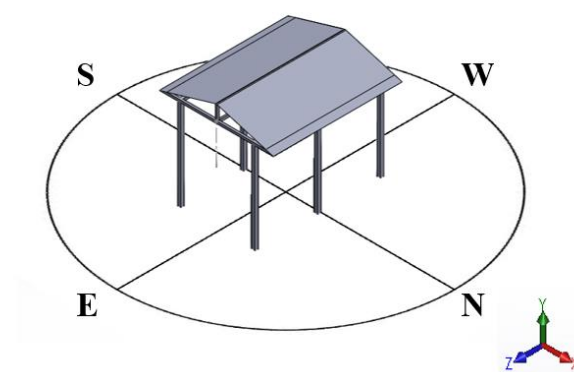


Figure 3.3: Orientation of the dryer

In this study, three GHSDs with different openings configurations were constructed to investigate the influence of openings arrangement on the microclimate of GHSD. Each GHSD has a hemispherical shape and it is covered with 0.2 mm thick polyethylene film. The GHSDs were labelled as G1, G2 and G3 respectively. G1 was totally enclosed without any openings. G2 has two openings with identical size of 1.1 m  $\times$  0.35 m on the east side at 1.85 m height (Figure 3.4). Besides, it has an opening on the west side with the size of 2.2 m  $\times$  0.3 m at 3.85 m height. The total openings area of G2 on the east and west sides were 0.77 m<sup>2</sup> and 0.66 m<sup>2</sup> respectively. G3 has an 2.6 m  $\times$  0.5 m opening on the east side and two 0.4 m  $\times$  3 m openings on the west side (Figure 3.5). Both of the east and west sides have an arc opening at the top. The height of the arc openings was 0.88 m. The total openings area of G3 on the east and west sides were 3.54 m<sup>2</sup> and 4.64 m<sup>2</sup> respectively.

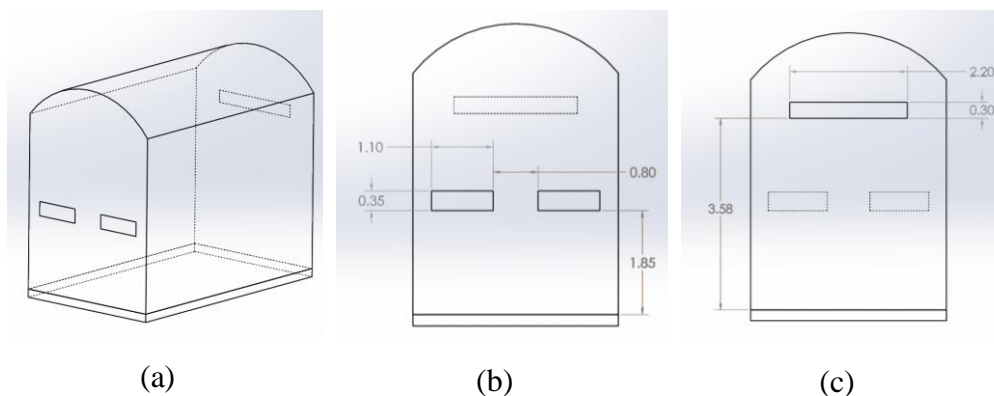


Figure 3.4: Opening configuration of G2 in (a) Isometric, (b) Front and (c) Back views

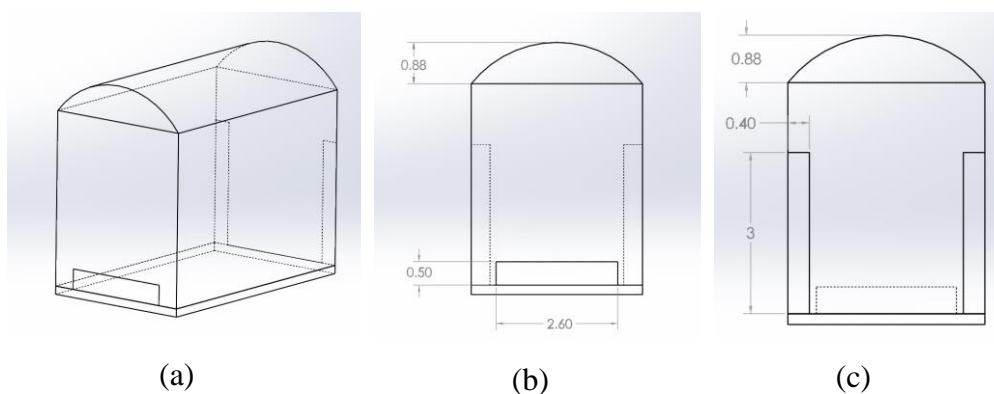


Figure 3.5: Opening configuration of G3 in (a) Isometric, (b) Front and (c) Back views

### 3.3 Mathematical Model and Governing Equations

The commercial CFD software, ANSYS Fluent 2021 R1 was used to study the microclimates within the dryers by using a finites volumes method to solve the governing equations for fluid flow and heat transfer. The governing equations for fluid flow are based on the three conservation laws which are the continuity, momentum and energy equations. The air flow within the dryers was assumed to be three-dimensional, steady state, incompressible, and turbulent. The governing equations are presented as follows:

Continuity equation:

$$\frac{\partial \rho \bar{u}_i}{\partial x_i} = 0 \quad (3.1)$$

Momentum equation:

$$\rho \bar{u}_j \frac{\partial \bar{u}_i}{\partial x_j} = -\frac{\partial \bar{p}}{\partial x_i} + \frac{\partial}{\partial x_j} \left[ \mu_t \left( \frac{\partial \bar{u}_i}{\partial x_j} + \frac{\partial \bar{u}_j}{\partial x_i} \right) \right] \quad (3.2)$$

Energy equation:

$$\rho \bar{u}_j \frac{\partial \bar{T}}{\partial x_j} = \frac{\partial}{\partial x_j} \left[ \left( \frac{\mu_l}{\sigma_l} + \frac{\mu_t}{\sigma_t} \right) \frac{\partial \bar{T}}{\partial x_j} \right] \quad (3.3)$$

The effect of turbulence on the air flow within the dryer was solved by using the  $k$ - $\varepsilon$  realizable model. The  $k$ - $\varepsilon$  realizable model was found to be able to obtain a better predictions of the air flow distribution compared to  $k$ - $\varepsilon$  standard model (Kim et al., 2008). It is a semi-empirical model subject to transport equations for the turbulent kinetic energy and turbulent dissipation rate. The model is applicable to analyse turbulent flows in a wide enclosure.

Turbulent kinetic energy ( $k$ ) equation:

$$\rho \bar{u}_j \frac{\partial k}{\partial x_j} = \frac{\partial}{\partial x_i} \left( \frac{\mu_t}{\sigma_k} \frac{\partial k}{\partial x_j} \right) + \mu_t \left( \frac{\partial \bar{u}_i}{\partial x_j} + \frac{\partial \bar{u}_j}{\partial x_i} \right) \frac{\partial \bar{u}_i}{\partial x_j} - \rho \varepsilon \quad (3.4)$$

Turbulent kinetic energy dissipation ( $\varepsilon$ ) equation:

$$\rho \bar{u}_j \frac{\partial \varepsilon}{\partial x_j} = \frac{\partial}{\partial x_j} \left( \frac{\mu_t}{\sigma_\varepsilon} \frac{\partial \varepsilon}{\partial x_j} \right) + C_1 \mu_t \frac{\varepsilon}{k} \left( \frac{\partial \bar{u}_i}{\partial x_j} + \frac{\partial \bar{u}_j}{\partial x_i} \right) \frac{\partial \bar{u}_i}{\partial x_j} - C_2 \rho \frac{\varepsilon^2}{k} \quad (3.5)$$

### 3.4 Radiation Model

Solar radiation is the important heat source that provides heat to the dryers to perform the drying process. It affects the air temperature and air flow distribution within the dryers. Therefore, a radiation model was applied into the CFD simulations to simulate the effect of solar incident irradiance on the dryers. The DO model was selected with the application of solar ray tracing method. It was recommended for solving the solution of radiation in semi-transparent materials and it was widely applied in simulating the effect of solar radiation on the air domain within a GHSD. The DO model solves the radiative transfer equation. The radiative transfer equation is presented as below:

$$\begin{aligned} \nabla(I(\vec{r}, \vec{s})\vec{s}) + (\alpha_\lambda + \sigma_s)I(\vec{r}, \vec{s}) &= \alpha_\lambda n^2 \frac{\sigma T^4}{\pi} \\ &+ \frac{\sigma_s}{4\pi} \int_0^{4\pi} I(\vec{r}, \vec{s}') \Phi(\vec{s} \cdot \vec{s}') d\Omega' \end{aligned} \quad (3.6)$$

Where  $\vec{r}$  is the position vector,  $\vec{s}$  is the direction vector,  $\vec{s}'$  is the scattering direction vector,  $I$  is the radiation intensity ( $\text{W}/\text{m}^2$ ) in the position ( $\vec{r}$ ) and direction ( $\vec{s}$ ),  $s$  is the stroke length (m),  $\alpha_\lambda$  is the absorption coefficient,  $\sigma_s$  is the scattering coefficient,  $n$  is the refractive index,  $\sigma$  is the Stefan-Boltzmann constant ( $5.669 \times 10^{-8} \text{ W}/\text{m}^2 \cdot \text{K}^4$ ),  $T$  is the temperature (K),  $\Phi$  is the phase function and  $\Omega'$  is the solid angle. The wavelength of solar radiation varies between 0.2 and 3  $\mu\text{m}$  (Kim et al., 2008). In order to simplify the simulation, the refractive index, absorption and scattering coefficients were assumed independent of wavelength.

The geographical location, mesh orientation, time zone, sunshine factor and time of the day were imported to the solar ray tracing model to calculate the illumination parameters and sun direction vector by using solar calculator in Fluent. A fair weather condition was defined in the solar calculator. In this study, the solar radiation on 10 February 2022 at 1.00 PM was considered



as input to solar ray tracing model. The spectral absorption coefficient,  $\alpha_\lambda$  of the participating media can be calculated from the its absorptivity,  $\alpha$  and thickness,  $d(\text{m})$ . The relationship between the absorption coefficient and absorptivity is presented in the equation as below:

$$\alpha_\lambda = \frac{1}{d} \ln \left( \frac{1}{1-\alpha} \right) \quad (3.7)$$

### 3.5 Species transport model

The species transport model was enabled in order to investigate the RH distribution within the dryers. The conservation equation are able to be solved with this model in a turbulent flow for the convection, diffusion and reactions of each species in mass fractions specified by the user in the mathematical model (Villagran et al., 2020). After the species transport model has been enabled, a mixture template was created with the mixture of air and water vapor to represent the moisture in the air. The mass fraction of the input species can be predicted from the following equation in a CFD model:

$$\nabla(\rho Y_i) = -\nabla J + N_i + E_i \quad (3.8)$$

Where  $Y$  is the local mass fraction of water vapor from the diffusion-convection equation,  $J$  is the water vapor diffusion flow,  $N_i$  is the production rate of the water vapor in component  $i$  and  $E_i$  is the moisture source term.

### 3.6 Computational domain and mesh generation

The stages that consist of the modelling of the computational domain, defining the boundary conditions, and selecting the size and type of meshing of the domain are the main and important parts in conducting CFD simulations. In order to obtain a more realistic air flow pattern over and within the dryers, the simulation of the coupling effect between the internal and external environments was considered in this study. The dominant wind direction of the site was reported from East (Weatherspark, 2022). Therefore, a windward and leeward were defined at the east and west sides respectively. Furthermore, no load

condition was considered where the samples of paperboard to be dried were not included in the dryers to simplify the mathematical models.

The coupled three-dimensional computational domain was constructed which includes both the inner and outer region of the dryers. The outer region of the dryers is defined as atmospheric boundary layer (ABL). In order to prevent any potential reversed flow and unnatural air flow that caused by the atmosphere boundary layer walls from interfering with the air flow around and in the dryers, the computational domain has to be large enough to capture an acceptable prediction of the airflow inside the ABL. However, large domains are expensive in terms of computational cost. Therefore, a proper domain size was obtained based on the recommendation from the research carried out by Li et al. (2020). The maximum height,  $H$  of the dryers were used to determine the size of the computational domain. The distance of the external flow field including windward, upper border and leeward from the dryers were defined at  $6H$ ,  $5H$  and  $15H$  respectively (Figure 3.6). Thus, the dimensions of the computational domain were 65.82 m, 31.28 m and 114.88 m in the length, width and height respectively.

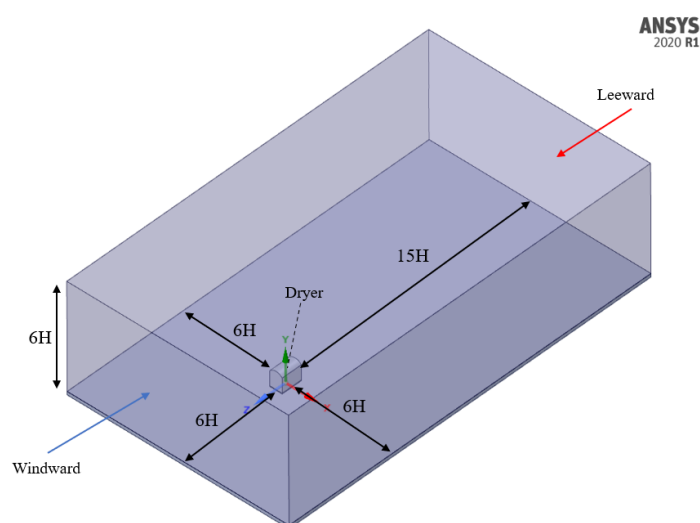
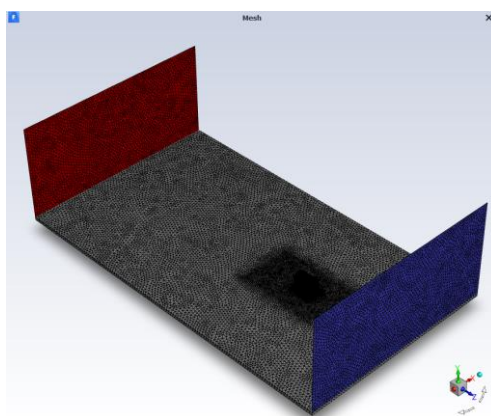


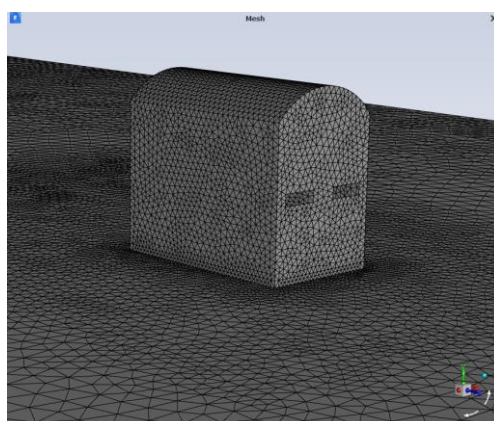
Figure 3.6: Computational domain for simulation

The geometry of the dryers were constructed in Solidworks and imported into ANSYS Workbench. The ABL domain was created as an enclosure around the dryers using SpaceClaim. Shared topology was enabled to achieve a conformal mesh. The meshing of the models was performed using the

Fluent Meshing tools. There were four cell zones created in each model which are the ABL domain, dryer domain, dryer floor and ground. The unstructured tetrahedron mesh with 1.1 cell growth rate was applied to all of the created zones and surfaces of the model. The patch conforming method was applied to the dryer domain and floor to improve the mesh quality. The mesh size of the ABL and ground was globally defined in a range of 900 to 2000 mm. The mesh sizes of the dryers and the floor were defined at 200 mm and 150 mm respectively with soft behaviour (Figure 3.7). A boundary of influence (BOI) with a size of  $15.8 \text{ m} \times 10 \text{ m} \times 25 \text{ m}$  was created within the computational domain which intersects between the dryers and ABL as shown in Figure 3.8. The element size of BOI was defined at 400 mm to create local mesh refinement in the intersection region. This feature was used to avoid the selected mesh sizes not being recorded, due to the large difference between the mesh sizes of ABL and dryer domains.

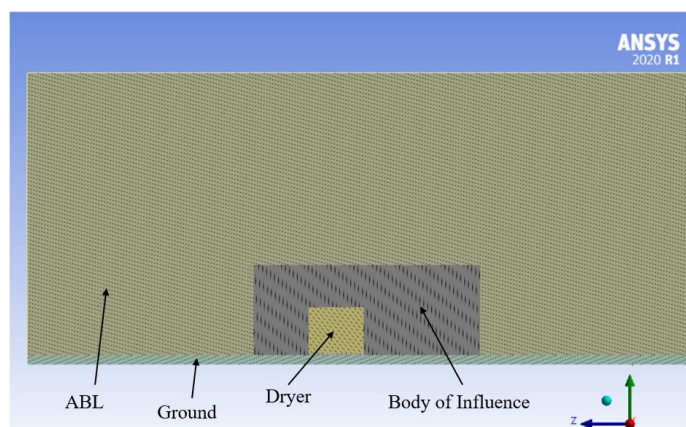


(a)

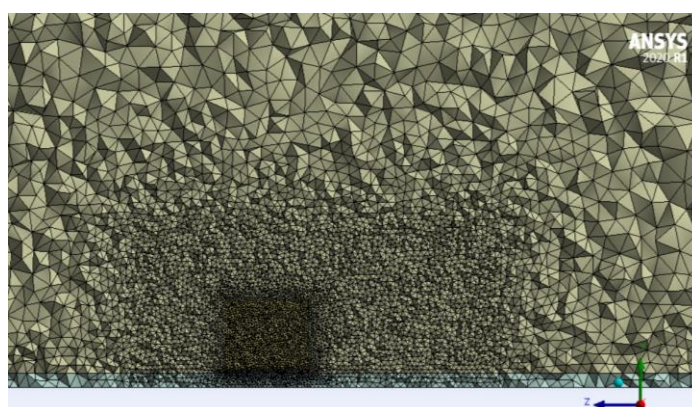


(b)

Figure 3.7: Meshing of (a) Computational domain and (b) Dryer



(a)



(b)

Figure 3.8: Cross sectional view of (a) Geometry and (b) Mesh of BOI

The quality of the generated mesh was evaluated from the mesh metrics including the parameter of the orthogonality, skewness, aspect ratio and Jacobian ratio (Zhang et al., 2019). The mesh result is shown in Figure 3.9. The minimum orthogonal quality was 0.27 which falls in the favourable range of 0.20 to 0.69. The maximum skewness of the mesh was 0.76. Skewness is the most used parameter in various studies to determine the mesh quality. The smaller the skewness value indicates the better mesh quality. According to the ANSYS Fluent Manual (Ansys Fluent, 2013), a maximum skewness value below 0.95 is recommended for mesh quality control. The maximum aspect ratio of the mesh was 8. The Jacobian ratio of the mesh was 1. The higher the value of Jacobian ratio indicates the higher distortion of the created mesh. After the mesh has been updated to the Fluent, meshing checking was conducted to ensure there is no negative volumes error to avoid any calculation error during the solution process.

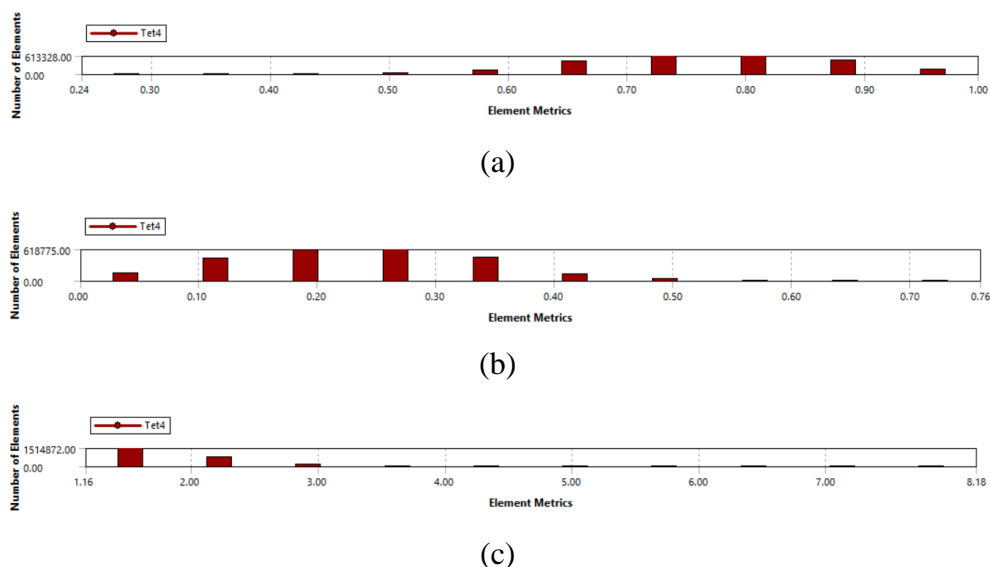


Figure 3.9: Mesh metrics (a) Orthogonality, (b) Skewness and (c) Aspect ratio

### 3.7 Boundary conditions

For solving any CFD problems, boundary conditions are needed to be defined. Boundary conditions are required in solving mathematical model as they have great influence to the fluid flow which results a unique solution (Duong et al., 2021). In the computational domain, the windward surface was set as velocity inlet where the direction of the wind was normal to the boundary. The wind speed of 1.8 m/s at a reference height of 10 m was considered in this study (Swarno et al., 2020). The wind was defined to enter the domain with a logarithmic velocity profile to represent a realistic atmospheric condition (Figure 3.10). The logarithmic velocity profile was calculated through the equations as below (Richards and Hoxey, 1993):

Velocity profile:

$$u(z) = \frac{u_*}{\kappa} \ln \left( \frac{z+z_0}{z_0} \right) \quad (3.9)$$

Turbulent kinetic:

$$k = \frac{u_*^2}{\sqrt{c_\mu}} \quad (3.10)$$

Epsilon:

$$\varepsilon = \frac{u_*^3}{\kappa(z+z_0)} \quad (3.11)$$

Where  $u_*$  is friction velocity (m/s),  $u(z)$  is velocity (m/s) at height  $z$  (m),  $\kappa$  is the von Karman's constant ( $\kappa = 0.42$ ),  $C_\mu$  is the constant fitting parameter ( $C_\mu = 0.09$ ),  $z_0$  is the surface roughness coefficient length (m) which was selected at 0.2 m based on the landscape type (Bañuelos-Ruedas, Angeles-Camacho and Rios-Marcuello, 2010). The turbulence distribution at the inlet was specified by turbulent kinetic energy and dissipation rate which were defined as the functions of  $u_*$ . The velocity profile and turbulence distribution were defined using User-Defined Function (UDF). The UDFs were constructed in the C programming language with the DEFINE macros provided by Fluent and interpreted in the setup. The leeward surface of the computational domain was set as a pressure outlet with 0 Pa gauge pressure. The air temperature and relative humidity entering from the inlet and outlet were set at 31 °C and 80 % which represent the ambient air temperature and humidity around the dryers (Tham et al., 2017).

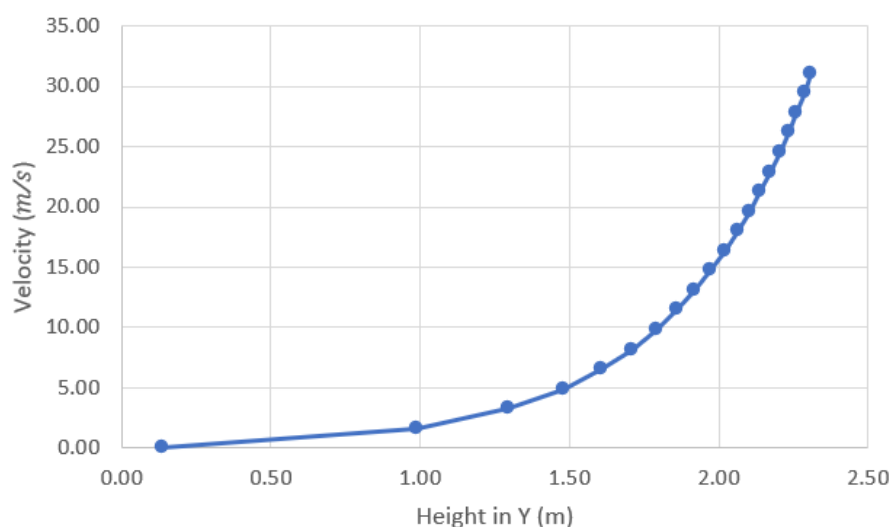


Figure 3.10: Logarithmic wind velocity profile

The top and the side surfaces of the computational domain which are parallel to the inlet air flow were set as symmetry boundaries to prevent any influence to the dynamics of the air flow due to friction loss. The roof of the open-shed dryer, cover of the GHSDs, ground and floor of the dryers were defined as wall type boundaries. The roof of the open-shed dryer was surrounded by a fluid region. It was defined as a two-sided wall boundary. Therefore, a coupled wall condition was selected in order to couple the thermal condition and a shadow wall was automatically created by the Fluent. There was no additional input thermal conditions are needed as the Fluent solver will be directly solving the conduction, convective and radiation heat transfer from the solution in the adjacent cells. The material of the roof was selected as zinc sheet with 0.001 m thickness. The emissivity and absorptivity were set to 0.25 and 0.3 respectively. It was enabled as opaque medium under the solar boundary condition.

The plastic film cover of the GHSDs was also defined as a coupled two-sided wall boundary as it was in between of the external flow field air domain and air domain within the dryer. Polyethylene was set as the material of the cover. The thickness of the cover was set to 0.0002 m. The emissivity, absorptivity and transmittivity of the cover were set to 0.7, 0.1 and 0.75 respectively at the shadow wall which is adjacent to the fluid region. The cover was enabled as semi-transparent medium under the solar boundary condition. The openings of the GHSDs were set as interior type boundaries in order to allow the interactions between the fluid of the outer and inner regions of the dryers. The floor surface of the dryers were defined as coupled wall as they were the junction surface between the solid and fluid region. The thickness of the surfaces were not required as the floor was modelled in a solid cell zone. The emissivity and absorptivity of the floors were set to 0.75 and 0.45 respectively. The material of the floor surface was assigned as concrete and they were enabled as opaque medium under the solar boundary condition. The top surface of the ground around the dryers was set as coupled wall boundary. The emissivity and absorptivity of the ground were set to 0.9 and 0.5 respectively. The side and bottom surfaces of the ground were set as adiabatic walls (Li et al., 2020). The ground surface were set at zero thickness as it was already modelled as a solid

cell zone. The material of the ground surface was set as dry soil and they were enabled as opaque medium under the solar boundary condition.

All of the solid cell zones including the floor and ground were disabled from the participation in radiation due to their opaque materials (Ansys Fluent, 2013). The fluid cell zones of the ABL and dryers were enabled in the participation in radiation to solve for the radiation in the cell zones of the fluid domains. The thermo-physical and optical properties of the materials were adopted from Mesmoudi, Meguellati and Bournet (2017) and Villagrán and Bojacá (2020). The boundary conditions are summarized in Table 3.3.

Table 3.1: Optical properties of materials

<b>Material</b>	<b>Absorptivity</b>	<b>Scattering coefficient (1/m)</b>	<b>Refractive index</b>	<b>Emissivity</b>
<b>Zinc Sheet</b>	0.16	1	1	0.9
<b>Polyethylene film</b>	0.09	0	1.7	0.7
<b>Concrete</b>	0.6	1	1	0.75
<b>Dry soil</b>	0.5	1	1	0.9
<b>Air</b>	0.1	0	0	-

Table 3.2: Physical properties of materials

<b>Material</b>	<b>Density (kg · m<sup>-3</sup>)</b>	<b>Specific heat capacity (J/kg · K)</b>	<b>Thermal conductivity (W/m · K)</b>
<b>Zinc sheet</b>	7140	390	116
<b>Polyethylene film</b>	923	2300	0.34
<b>Concrete</b>	2100	910	1.5
<b>Dry soil</b>	1300	800	1
<b>Air</b>	1.225	1006.43	0.0242



Table 3.3: Boundary conditions

<b>Boundary name</b>	<b>Boundary type</b>	<b>Parameter</b>	<b>Value</b>
<b>Windward surface</b>	Velocity inlet	Velocity	1.8 m/s (z = 10 m)
<b>Leeward surface</b>	Pressure outlet	Pressure	0 Pa
<b>Top and side domain surfaces</b>	Symmetry	-	-
<b>Roof of open-shed dryer</b>	Coupled wall	Absorptivity Emissivity	0.25 0.3
<b>Cover of GHSDs</b>	Coupled wall	Absorptivity Transmissivity Emissivity	0.1 0.75 0.7
<b>Openings of GHSDs</b>	Interior	-	-
<b>Floor surfaces of dryers</b>	Coupled wall	Absorptivity Emissivity	0.45 0.75
<b>Top ground surface</b>	Coupled wall	Absorptivity Emissivity Roughness	0.5 0.9 0.2 m
<b>Side and bottom ground surfaces</b>	Adiabatic wall	Heat flux	0 W/m <sup>2</sup>

### 3.8 Numerical method

In this study, a steady-state approach was adopted as it was widely applied in various studies in investigating the microclimate within the dryers which helps in analyzing and predicting the drying performance of the dryers in terms of air flow pattern, temperature and RH distribution. Besides, steady-state simulation is useful in evaluating different opening configurations and geometries of the GHSDs in order to determine the most optimal design (Villagran, Henao-Rojas and Franco, 2021). Furthermore, a simple transient simulation was performed in this study to investigate the heat retention of the floor in the dryers.

The SIMPLE algorithm for pressure-linked equations was selected in the Fluent solution method to solve the pressure-velocity coupling equations.

Least square cell-based method was adopted to compute the gradient. A second-order upwind discretization scheme was selected for the momentum, energy and water vapor terms. The turbulent kinetic energy, turbulent dissipation rate and DO transport terms were defined to first order upwind discretization scheme (Li et al., 2020). The underrelaxation factors of momentum, pressure, turbulent kinetic energy and turbulent dissipation rate were set as 0.7, 0.3, 0.8, 0.8 respectively while the other factors were set as 1. The residual convergence criteria of energy and DO-intensity equations were set as  $1 \times 10^{-6}$  and  $1 \times 10^{-3}$  was set for the continuity and turbulence equations. The simulation models were solved using Intel(R) Core(TM) i5-7200U CPU @ 2.50 GHz processors with 8GB RAM.

Table 3.4: The settings of CFD simulation

<b>Classification</b>	<b>Setting of method</b>
<b>Solver</b>	3D simulation Implicit formulation Absolute velocity formation Steady state analysis
<b>Energy equation</b>	Activated
<b>Viscous model</b>	Realizable $k$ - $\varepsilon$ model Standard wall function
<b>Radiation model</b>	Discrete ordinates (DO) model Theta divisions: 2 Phi divisions: 2 Theta pixels: 1 Phi pixels: 1 Non-grey model: non selected Iteration ratio (flow/radiation): 10
<b>Species model</b>	Multiple species
<b>UDF</b>	DEFINE Profile
<b>Timestep size (for transient)</b>	10 s

## CHAPTER 4

### RESULTS AND DISCUSSION

#### 4.1 Introduction

The CFD simulations were performed to study the microclimate of open-shed and GHSDs with different opening configurations. In this section, the results obtained from the CFD simulations including the distributions of air temperature, velocity and RH within the dryers were presented in figures and graphs. The results were analysed to discuss the comparison between open-shed dryer and GHSD. Besides, the results were also used to evaluate the effect of opening configurations on the microclimate within the GHSDs. Lastly, an optimized design of dryer was proposed based on the evaluated results and the improvement in drying performance provided by the proposed design were discussed in this section.

#### 4.2 Selection of planes and lines

In order to evaluate and visualize the distributions of air temperature, velocity and RH within the dryers, the contours were plotted in figures. There were three cross sectional planes were selected in X, Y and Z axes of each dryer to plot the contours. All of the planes were located at the centre of each dryer. Based on the global coordinate of the dryers, the planes were located at 0, 2.59 and 0 in X, Y and Z axes respectively. However, only the contour plot of planes in X axis and graph plot of lines in Y axis were used in discussion. The contours and graphs in other planes and lines were included in appendix. Furthermore, the distributions of air temperature, velocity and RH in each dryer were plotted in graphs. There were two lines constructed along Y and Z axes of each dryer to plot the graphs. The line in Y axis was located at the centre of the dryers and the line Z axis was located at  $Y = 2.59$  m. The selected planes and lines were illustrated in Figure 4.1.

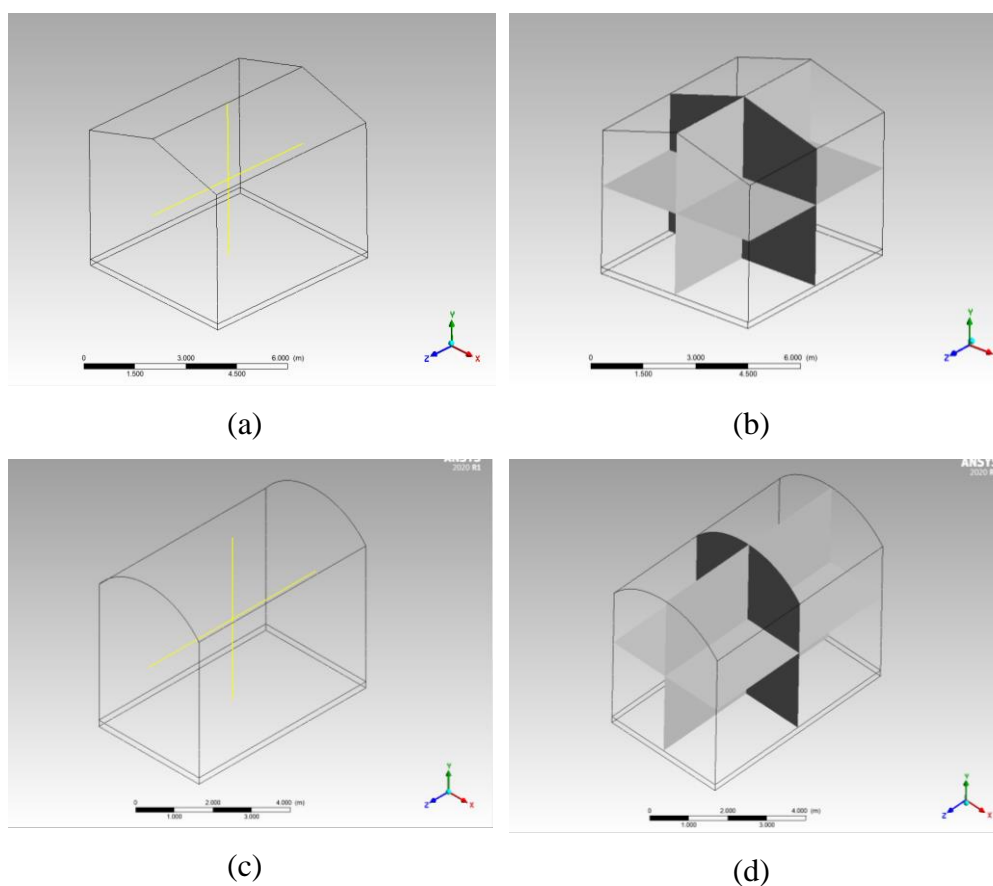


Figure 4.1: Selected lines and planes of ((a) and (b)) Open-shed and ((c) and (d)) GHSDs

### 4.3 Air flow distribution

Air flow was determined as one of the main factors in affecting the drying rate of a product. Many researchers have investigated the influence of air flow on the drying rate of different product. It was reported that an optimum velocity of air flow around the drying products were able to improve the drying rate. Besides, a proper air flow could prevent the accumulation of moisture around the drying products. The air velocity contours in open-shed, G1, G2 and G3 were presented in Figure 4.2. The vector of the air flow in open-shed, G1, G2 and G3 were illustrated in Figure 4.3 to visualize the air flow distribution in the dryers.

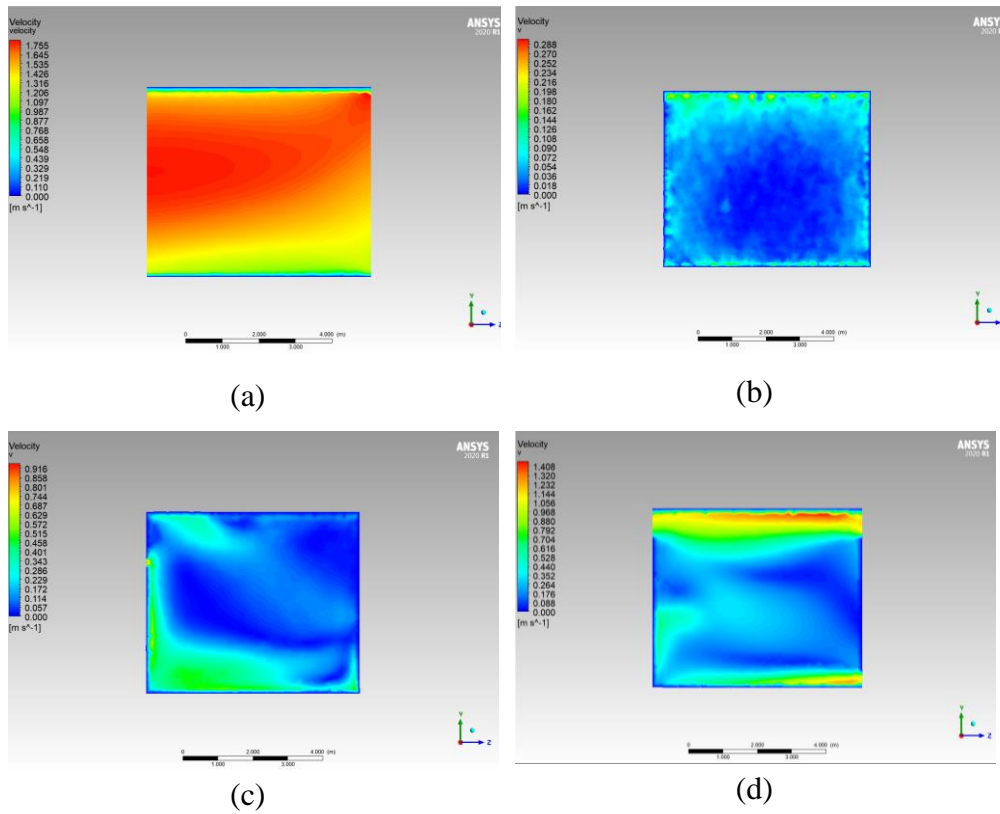


Figure 4.2: Side view of velocity magnitude in (a) Open-shed dryer, (b) G1, (c) G2 and (d) G3

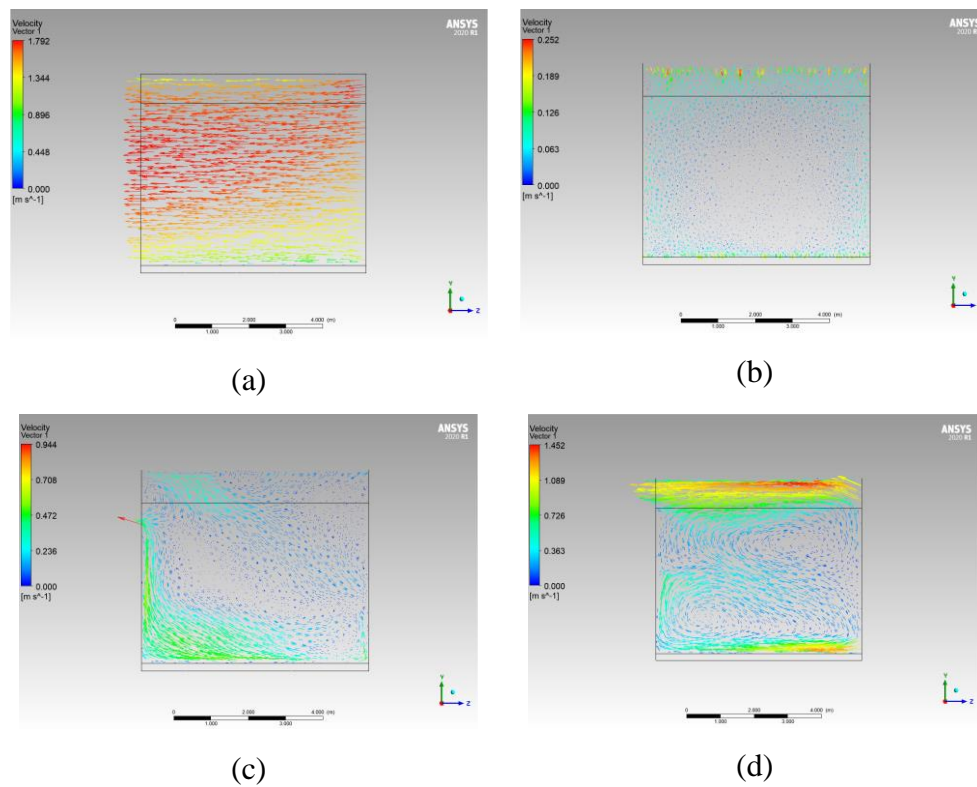


Figure 4.3: Side view of velocity vector in (a) Open-shed dryer, (b) G1, (c) G2 and (d) G3

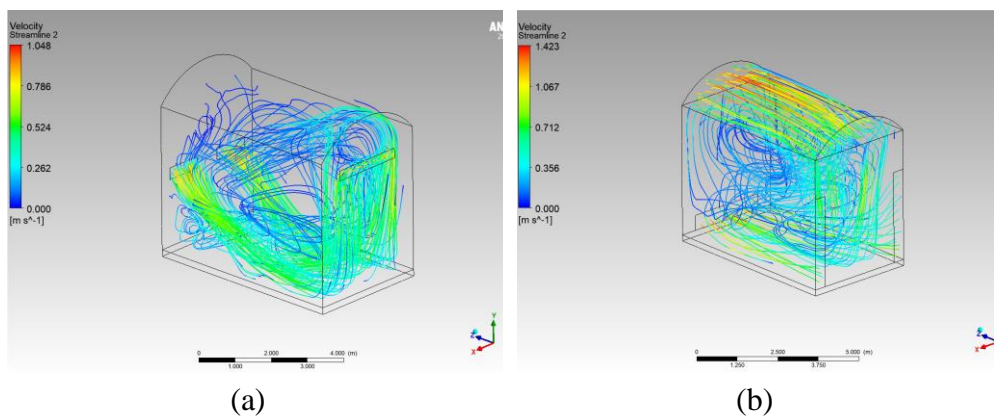


Figure 4.4: Isometric view of air flow streamlines in (a) G2 and (b) G3

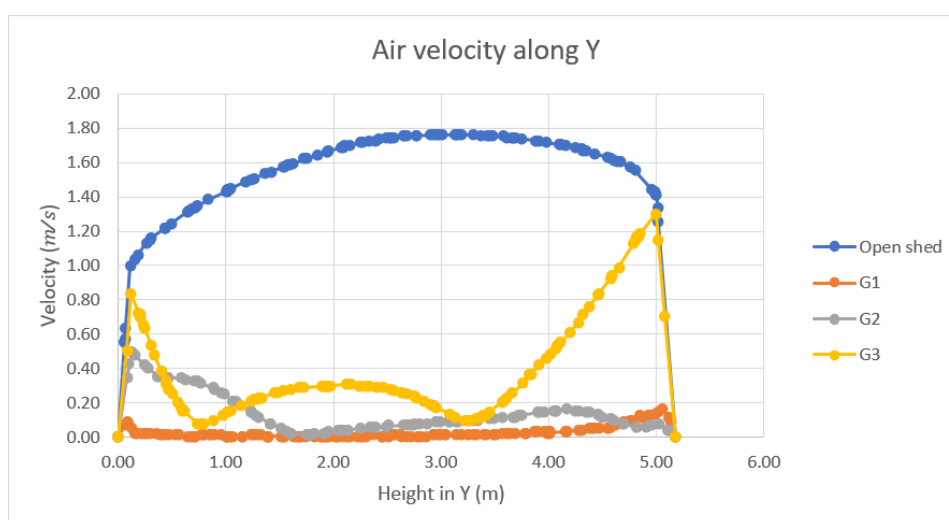


Figure 4.5: Graph of air velocities along the height in Y

From the velocity contours of open-shed dryer (Figure 4.1(a)), the air flowing into the dryer with a velocity profile (0.64 – 1.76 m/s) along the height can be observed at the east region of the dryer. The air in external environment was flowing with a logarithmic profile. Hence, the air entering the open-shed dryer has the similar profile as the external environment. However, the velocity profile was not consistent along the length of the dryer in Z axis. This phenomena can be explained due to the non-slip boundary of the roof surface. The non-slip boundary reduced the air velocity near the surface and another velocity profile was developed. Thus, a forced flow was created onto the adjacent air flow and changes the velocity profile of the entering air.

For case of G1, G2 and G3, it can be observed that the air movement within the GHSDs was significantly reduced compared to open-shed dryer (Figure 4.2). The G1 is an enclosed cavity which has the minimum air

movement as the interaction of air between the internal and external environment was restricted. The air movement in the centre of G1 was found weak with low velocities. The air velocities near the cover and floor were relatively higher than the centre region of the dryer. The air movement near the cover and floor was thermally driven by the heat from the cover and floor. A similar result was observed by Tigampo et al. (2020) in their study.

The G2 and G3 have the similar ventilation style where the openings were located at the east and west sides of the dryers. The difference is the area of openings. The area of openings of G2 were  $0.77 \text{ m}^2$  and  $0.66 \text{ m}^2$  on the east and west sides respectively. G3 has larger area of openings than G2 which were  $3.54 \text{ m}^2$  and  $4.64 \text{ m}^2$  on east and west sides respectively. The openings allowed the air inside the dryer to interact with the external environment. Therefore, the streamlines of air flow in G2 and G3 were presented in Figure 4.4 to visualize the air flow within the dryers.

For the case of G2, it was observed that the air flowing into dryer through the openings on the east side (Figure 4.2(c)). The entering air flow went down to the floor area and flowing horizontally above the floor. The air was then moving upward and exist through the opening on the west side. The air movement in the bottom region near the floor was relatively strong with air velocities around  $0.5 \text{ m/s}$  compared to other regions in the dryer. The region at the center and upper east side of the dryer was found having a poor air movement with air velocities below  $0.2 \text{ m/s}$  and almost at rest. A similar air flow pattern was observed in the study by Villagran, Henao-Rojas and Franco (2021).

For the case of G3, it can be observed that the air movement in the dryer is stronger than G2 (Figure 4.5). High velocities of air flow were found at the top region near the roof due to the large openings located below the roof on the east and west sides of the dryer. The large openings allowed more air flowing across the region with higher air velocities around  $1.2$  to  $1.4 \text{ m/s}$ . Besides, the region near at the opening where the air enters has a relatively higher air velocities due to the stronger air movement of the entering air. There are two air circulation patterns were shown in the top and bottom regions of the dryer (Figure 4.3(d)). From the Figure 4.5, it was found that G3 has a better air flow than G2 in the region where Y in the range of 1 to 3 m.

The mass flow rates at the openings of G2 and G3 were computed by using the surface integral in Fluent. The mass flow rates of G2 and G3 were 0.68 and 3.64 kg/s respectively. A higher mass flow rate at the openings indicates a higher ventilation rate and air renewal between the internal and external environment of the GHSD (Flores-Velazquez et al., 2014). Hence, it can be concluded that the arrangement and areas of openings can be taken into consideration in optimizing the ventilation performance of a GHSD. Besides, it was also shown that GHSD is able to provide better control of airflow than open-shed dryer.

#### **4.4 Temperature distribution**

Air temperature is one of the most important factors in affecting the drying performance of a dryer. Many researchers have studied the effect of air temperature and drying curve in drying different products. It was found that higher temperature is able to improve the drying rate as the additional heat is able to enhance the evaporation of moisture content from the drying products. The air temperature contours in open-shed, G1, G2, and G3 are illustrated in Figure 4.6. The distribution of air temperature in the dryers along the selected line in Y axis was presented in Figure 4.7.

From the open-shed dryer temperature contour (Figure 4.6(a)), a small temperature gradient can be observed along the height of the dryer in Y axis. There was a slightly increment of temperature at the bottom region due to the heating from the warmer floor. However, the increment was low that the average temperature within the dryer was 33 °C which is close to the ambient temperature, 31 °C. The open-shed dryer is opened to the external environment. The large air flowing through the dryer constantly causes the high air exchange rate between the internal and external environment of the dryer. Thus, the temperature difference between inside and outside of open-shed dryer was low.



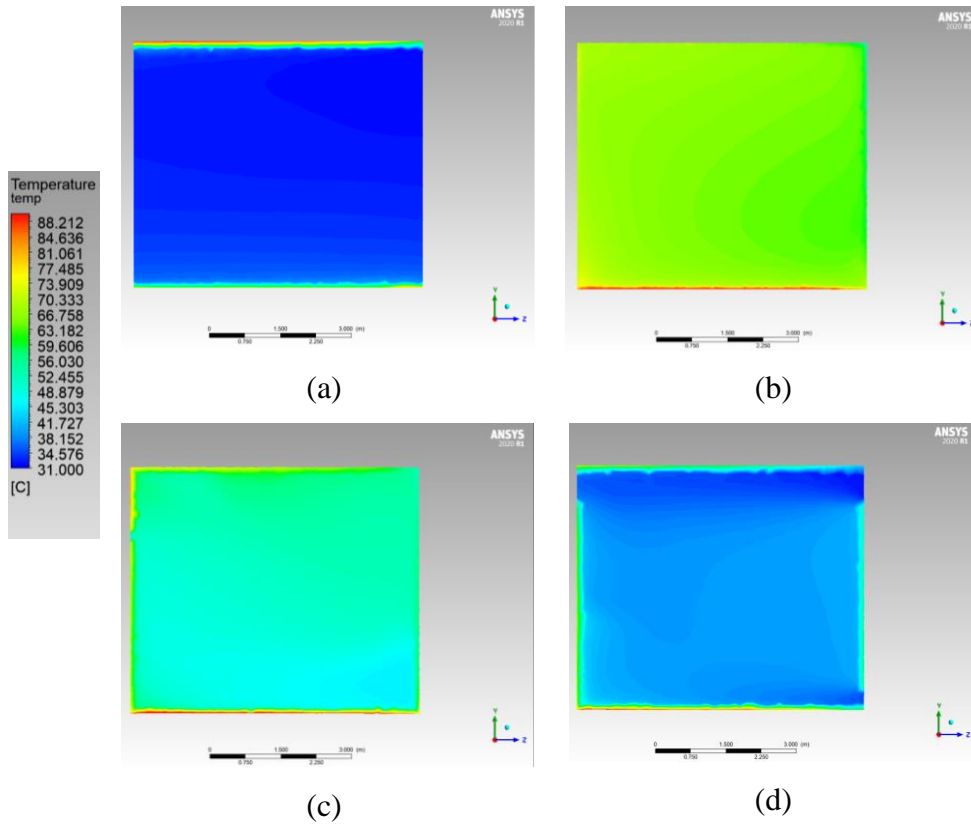


Figure 4.6: Side view of temperature distribution in (a) Open-shed dryer, (b) G1, (c) G2 and (d) G3

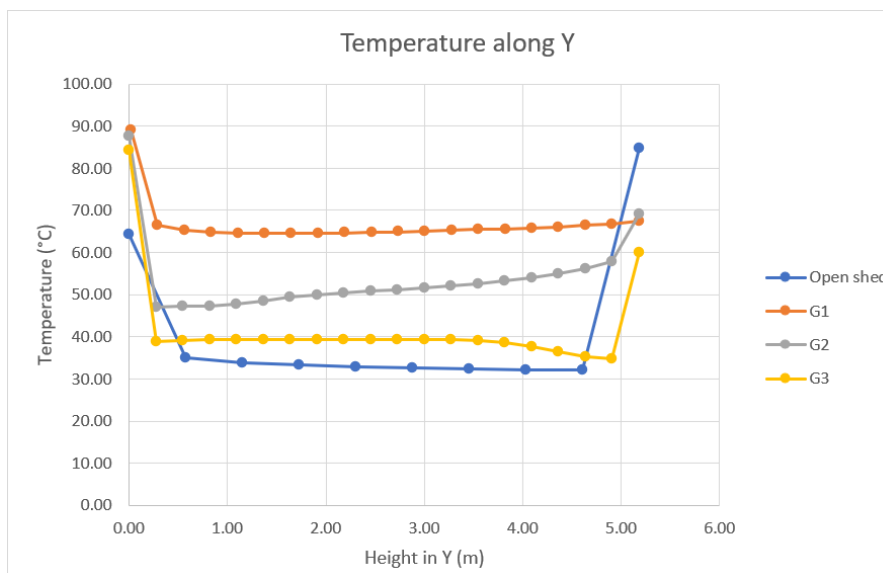


Figure 4.7: Graph of temperature along the height in Y

For the G1, G2 and G3, it can be observed that the GHSDs were able to provide a significant increment in temperature compared to the open-shed dryer (Figure 4.6). In the case of G1, the temperature within the dryer was

increased to about 63 to 67 °C. The temperature within the G1 was distributed evenly due to the totally enclosed environment without any openings on the dryer. The enclosed environment prevented interaction of the air between the internal and external environment of the dryer and therefore G1 was able to accumulate the heat in the drying space without any existence of air exchange with the external environment.

In the case of G2 and G3, it was obviously shown in the Figure 4.7 that both of the G2 and G3 have lower temperature than the G1. The temperature distribution in G2 along the height was in the range of 48 to 58 °C. From the temperature contour of G2 (Figure 4.6(c)), a lower temperature at 48 to 52 °C was observed at the bottom region of the dryer. The air flowing down towards the floor from the inlets caused the lower temperature in the bottom region due to the entering ambient air at lower temperature (31 °C). Besides, it was found that the temperature in the upper east region of G2 was higher due to the poor air flow in that region. This situation was found similar in the study by Senhaji, Mouqallid and Majdoubi (2019) that an obvious increment of temperature was found in poor air flow regions.

The G3 has the lowest temperature distribution inside the dryer compared to G1 and G2 due to the higher mass flow rate across the dryer. The temperature within the G3 ranged from 35 to 40 °C along the height (Figure 4.7). From the Figure 4.6(d), it can be observed that the temperatures in the regions near the roof and floor were lower than the middle region of the dryer. The temperature in the top region near to the roof was the lowest due to the large air flowing through which results in a higher air exchange in that region. The bottom region near to the floor has a lower temperature due to the location of the opening at the bottom of the east surface of G3. Besides, the temperature in the middle region (Y=1 to 3 m) of G3 has a better homogeneity than G2 due to the presence of air circulation in the region. The air circulation enhanced the air mixing and provides homogenous temperature distribution.

The average temperatures in the internal environment of the open-shed, G1, G2 and G3 were extracted by using volume integral in Fluent. The extracted average temperatures of open-shed, G1, G2 and G3 were 33.0, 65.6, 50.7 and 39.7 °C respectively. The G1, G2 and G3 was able to provide 6.7 to 32.6 °C higher temperature than open-shed dryer. The temperatures were found

reasonable based on the experiment by Janjai (2012) in Thailand. The GHSD investigated by Janjai was able to obtain drying temperatures varied from 35 to 65 °C. From these results, it can be conclude that GHSDs are able to achieve better drying performance than open-shed by providing higher drying temperatures. Besides, it was also found that the temperature profile within the GHSD was related to the area of openings and mass flow rate across the dryer. The higher mass flow rate results in lower drying temperature (Figure 4.8).

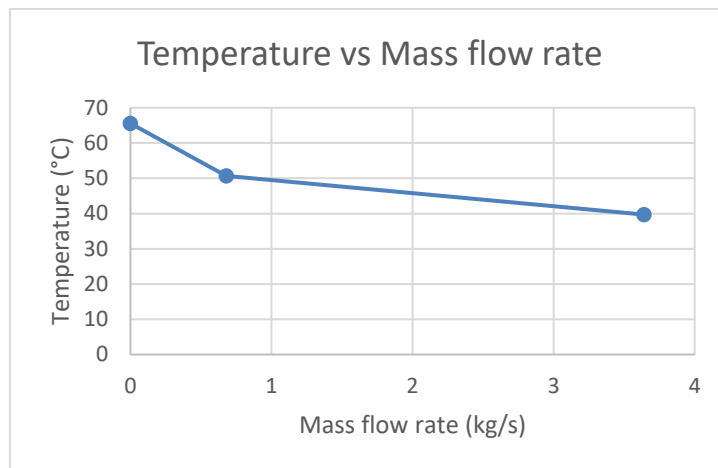


Figure 4.8: Graph of temperature against mass flow rate

#### 4.5 Relative humidity

Relative humidity (RH) is one of the main factors considered in this study to evaluate the drying performance of the dryers. As discussed in the previous section, RH is dependent on the air temperature. Many researchers have investigated the drying rates of products under different controlled RH values. It was reported that a lower RH is able to improve the drying rate by enhancing the moisture reduction from the product. The plotted RH contours of in the open-shed, G1, G2 and G3 were presented in Figure 4.9. The graph of RH distributions within the dryers along the selected line in Y axis was illustrated in Figure 4.10.

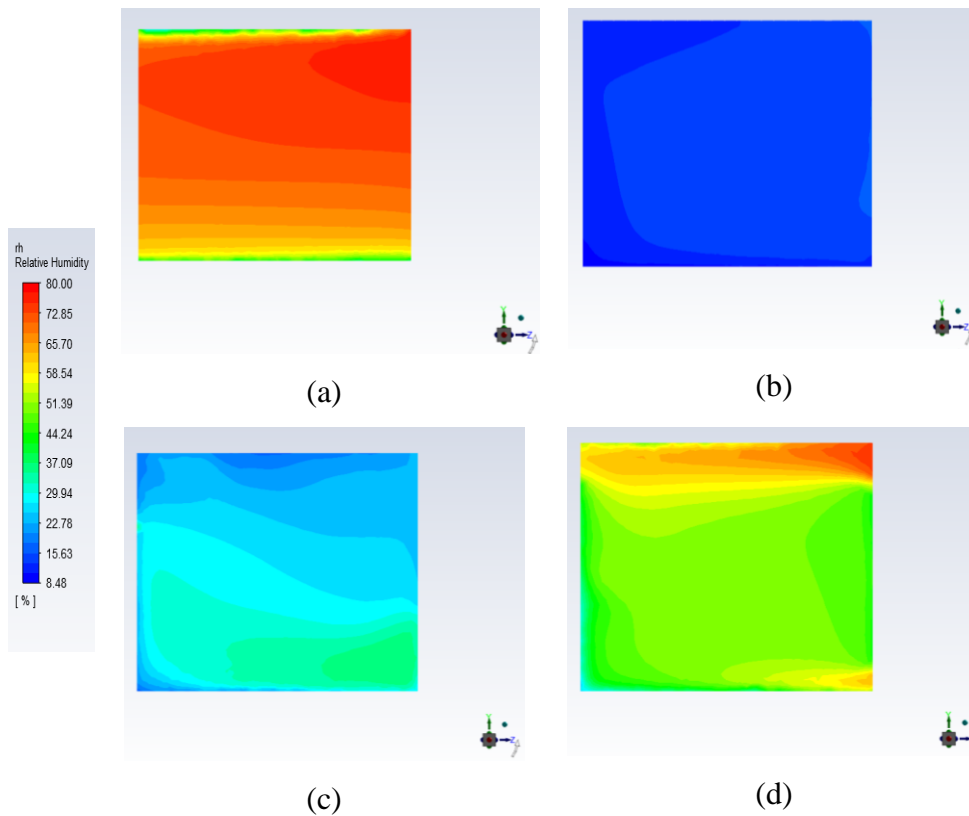


Figure 4.9: Side view of RH distribution in (a) Open-shed dryer, (b) G1, (c) G2 and (d) G3

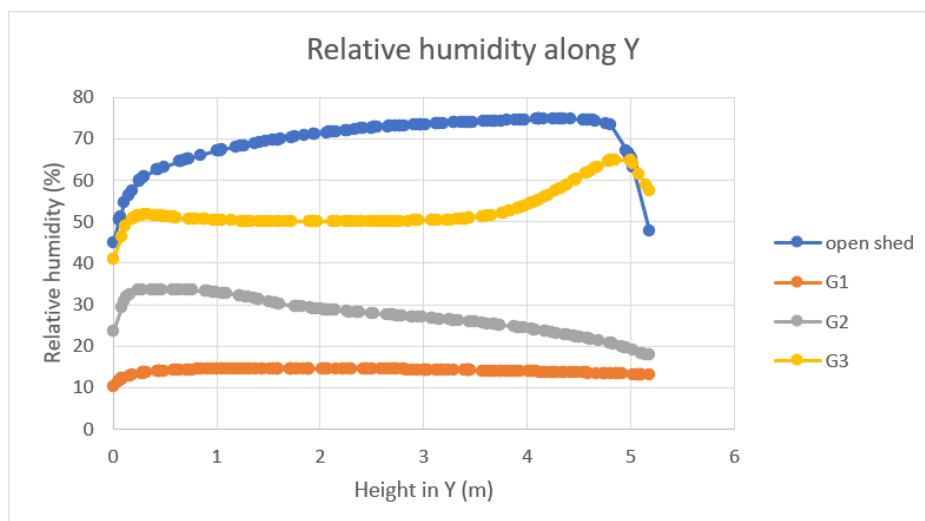


Figure 4.10: Graph of RH along the height in Y

From the RH contours (Figure 4.9) of the dryers including open-shed, G1, G2, and G3, it can be observed that the distributions of RH within every dryer were related to the temperature distributions. This phenomena can be explained due to the no load condition considered in this study. Without the

drying samples inside the dryers, the distribution of RH was limited to the psychrometric relation of the moist air to the temperature. Therefore, it can be observed from the RH contours that the regions with lower RH were found coincide with the regions of higher temperature. A similar results were obtained by Villagran et al. (2020) and Duong et al. (2021) in their studies.

In the open-shed dryer, the distribution of RH along the height in Y axis from bottom to top was varying from 46 to 75 % (Figure 4.10). The RH near the floor surface has the lowest RH due to the high temperature of the heated floor. Besides the RH near the roof was found low as 49 % due to the high temperature of the heated roof. The regions with high RH were due to the low temperature distribution which was caused by large air flow through the open-shed dryer. The ambient RH was 80 %. Thus, small RH differences were found between the internal and external environment of open-shed dryer.

From the RH contours of G1, G2 and G3, an obvious reduction in RH inside the GHSDs was observed compared to the open-shed dryer (Figure 4.9). In the case of G1, the RH was decreased to 14.6 %. It has the lowest values of RH distribution among the GHSDs. The RH was evenly distributed within the G1. The homogenous RH distribution was achieved due to the zero interaction of air between the internal and external environment of the dryer. Therefore, the homogeneity of the RH distribution in G1 was similar to its temperature homogeneity.

In the case of G2 and G3, it was shown in Figure 4.10 that higher RH values were found in both of the G2 and G3 compared to G1. The significant increment of the RH in G2 and G3 was caused by the increased air flowing into the dryers through the openings. The trend of RH distribution in G2 along the height in Y axis was different from G3. An increasing RH can be observed at the top region of G3 while a decreasing RH along the height was found in G2. The difference was caused by the different arrangement of openings on each dryer.

In the G2, the RH distribution within the dryer was found in the range of 18 to 33 % along the height (Figure 4.10). The higher RH values in the dryer were found in the lower region near the floor. This can explained due to the air flow pattern in that region. The ambient air flowing into the dryer sank to the floor area reduced the air temperature in the region near the floor. Thus, the RH

in the region was found higher due to the lower temperature. The region in the upper east of G2 has the lower RH due to the poor air flow and high temperature in the region.

For the case of G3, it can be observed that G3 has the highest RH values among the GHSDs (Figure 4.10). The RH values distributed along the height in G3 varied between 41 and 65 %. It was found that the RH in the top region has the higher values in G3. The high RH values at the top region was caused by the air flowing through the region as the large air flow from external environment reduced the air temperature in the region. Besides, a higher values of RH was found near the opening at the bottom of the east surface of G3 due to the lower temperature in the opening region.

Volume integral in Fluent was used to extract the average RH values in the open-shed, G1, G2 and G3. The average RH values in the open-shed, G1, G2 and G3 were 69.8, 14.1, 28.7 and 50.2 % respectively. The G1, G2 and G3 were able to provide 19.6 to 55.7 % lower RH than the open-shed dryer. Therefore, it can be concluded that GHSD was able to improve the drying rate from open-shed dryer by providing a drying environment with lower RH values. Furthermore, the RH distribution in a GHSD was found related to the opening configurations as the arrangement of openings affects the temperature distribution within the dryer.

#### **4.6 Thermal mass**

In this study, concrete was selected as the floor material to act as the thermal mass in the dryers. Concrete is a sensible heat storage materials which is commonly used in solar dryers due to its inexpensive cost and simple implementation. A simple transient CFD simulation was performed to investigate the heat retention of concrete and soil floor. The initial temperature of the floors was 50 °C and they were left to cool down for 1 hour and 30 minutes. The temperatures within the floor were plotted from bottom to the top surface (Y= 0 to 0.2 m) (Figure 4.11).

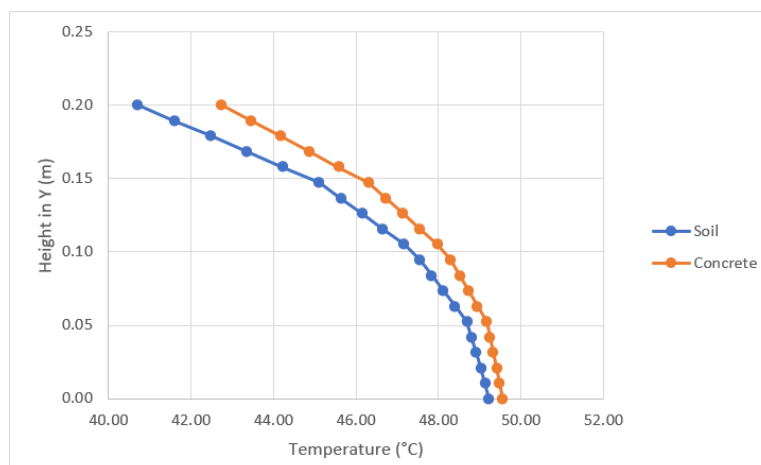


Figure 4.11: Temperature distribution in soil and concrete floor after 1 hour and 30 minutes of cooling

From the graph (Figure 4.11), it can be observed that the soil floor has lower temperature values than the concrete floor. The temperatures at the top surface of concrete and soil floor were 42.8 °C and 40.7 °C respectively. Therefore, it was found that the concrete floor was able provide better heat retention than the soil heat. The good heat retention allows the concrete floor to store the heat accumulated during the daytime and release it into the dryer after the sunset.

#### 4.7 Proposed design of dryer

The CFD simulations on the open-shed and GHSDs were performed study the distribution of air flow, temperature and RH inside the dryers. The analysis on the results has been done by evaluating the plotted contours and graph. It was found that GHSD is able achieve better drying performance than open-shed dryer by providing a more favorable drying environment including controlled air flow, higher temperature and lower RH. However, the drying performance of GHSD is not generalized as it could be affected by geometry, cover material and openings configuration.

In this study, the CFD simulations of GHSD models with different openings configurations were performed. Each model was found to have its advantage and disadvantage. G1 provided an enclosed environment that can retain the heat well and obtain high temperatures in the dryer. However, the air movement in G1 is very poor and this could cause the accumulation of moisture

in the environment while drying the paperboard. G2 has openings which act as the inlet and outlet to the air flowing through the dryer. It was able to provide higher drying temperature than ambient but lower than G1. The airflow in G2 is better than G1 but it has poor homogeneity. G3 has larger area of openings compared to G2. Thus, G3 has better air flow than G2. However, G3 has the lowest drying temperature due to the poor heat retention.

After evaluating the effect of openings on the drying environment of GHSD, a decision was made on optimizing the design of dryer to achieve a drying environment in between G2 and G3. The idea adopted in modifying the ventilation performance of the dryer was to implement mechanical ventilation with natural ventilation to achieve a compromise between the ventilation and heat retention performance. Therefore, besides of modifying the arrangement of openings, an exhaust fan was applied in the design. The proposed dryer with optimized design was labeled as G4. G4 has the same geometry which is a hemispherical shape and it is covered with 0.2 mm thick polyethylene film. The dimensions of G4 is 3.66 m (W)  $\times$  6.1 m (L)  $\times$  5.18 m (H) (Figure 4.12). An opening with an area of 0.78 m<sup>2</sup> was located on the east side at 1.85 m height. On the west side, a 0.5 m diameter exhaust fan with an air flow rate of 7240 m<sup>3</sup>/h. A concrete floor with 0.2 m thickness was implemented in G4.

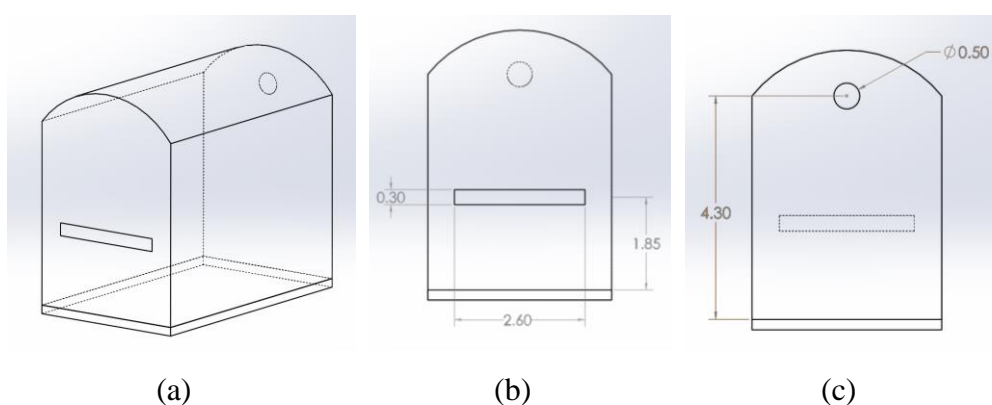
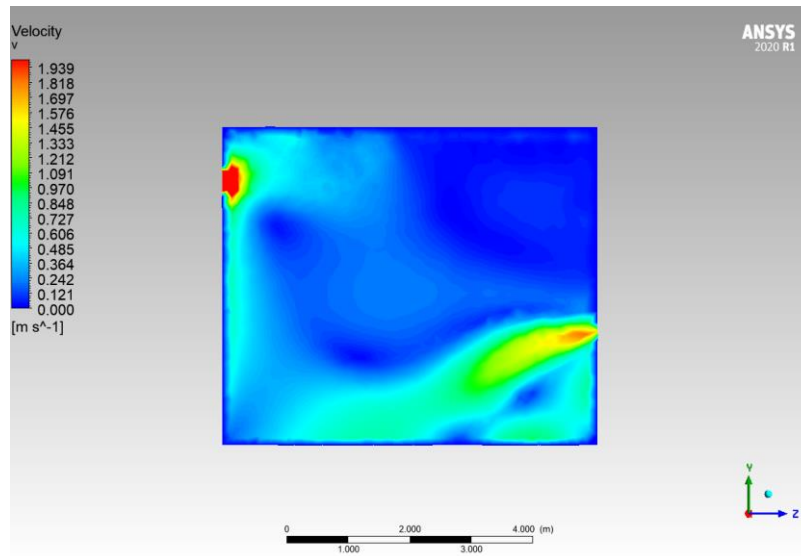


Figure 4.12: Opening configuration and location of exhaust fan on G4 in (a) Isometric, (b) Front and (c) Back views

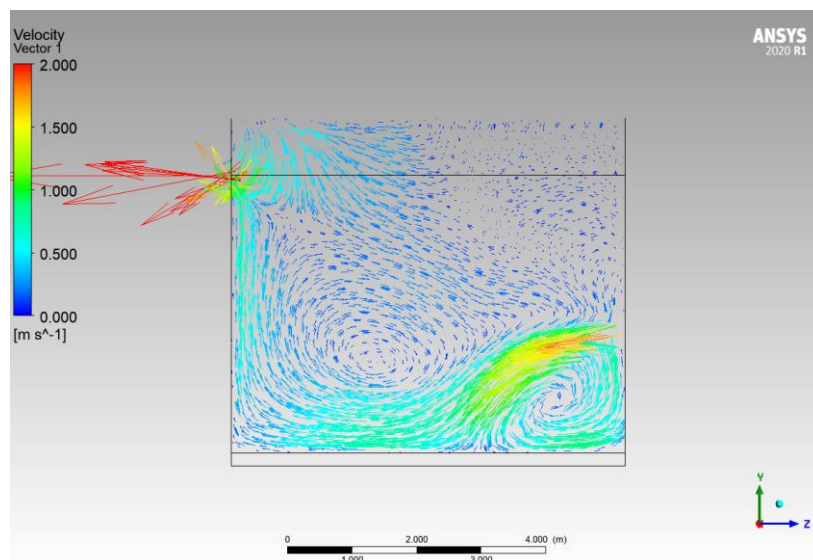
A steady state CFD simulation with the same meshing, procedure and solution method was performed to study the distribution of air flow, temperature and RH in G4. The same lines and planes in X, Y and Z axes was selected to



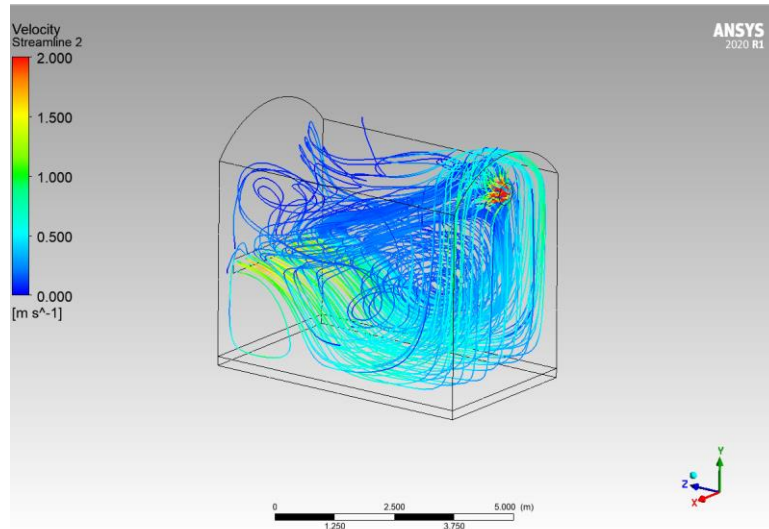
plot the contours and graphs. The contour, vector and streamlines distribution of air flow were illustrated in Figure 4.13. The contours of temperature and RH in G4 were presented in Figure 4.14. The graphs of the distribution of air velocity, temperature and RH along the height of G4 were shown in Figure 4.15. The results obtained in open-shed, G1, G2 and G3 were included in Figure 4.15 to show the difference and comparison.



(a)

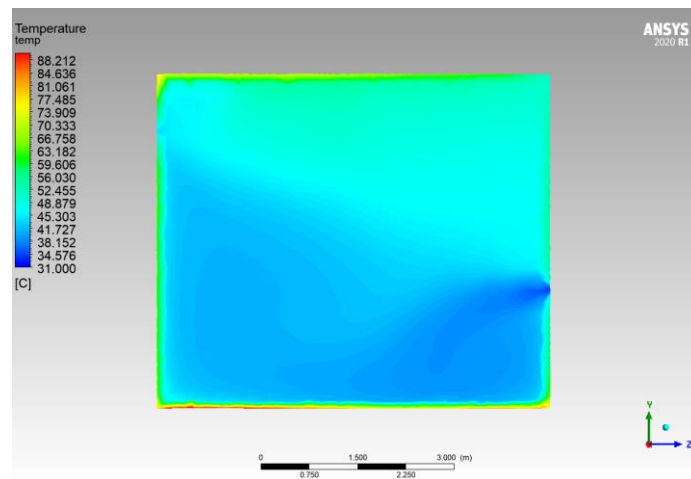


(b)

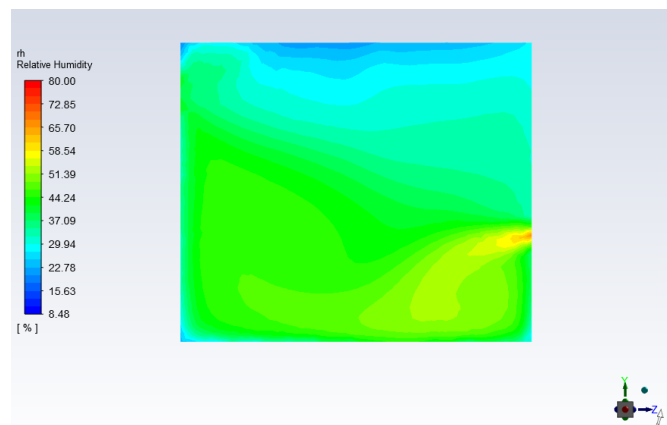


(c)

Figure 4.13: (a) Contour of velocity magnitude, (b) Velocity vector and (c) Air flow streamlines in G4



(a)



(b)

Figure 4.14: Contours of (a) Temperature and (b) RH in G4

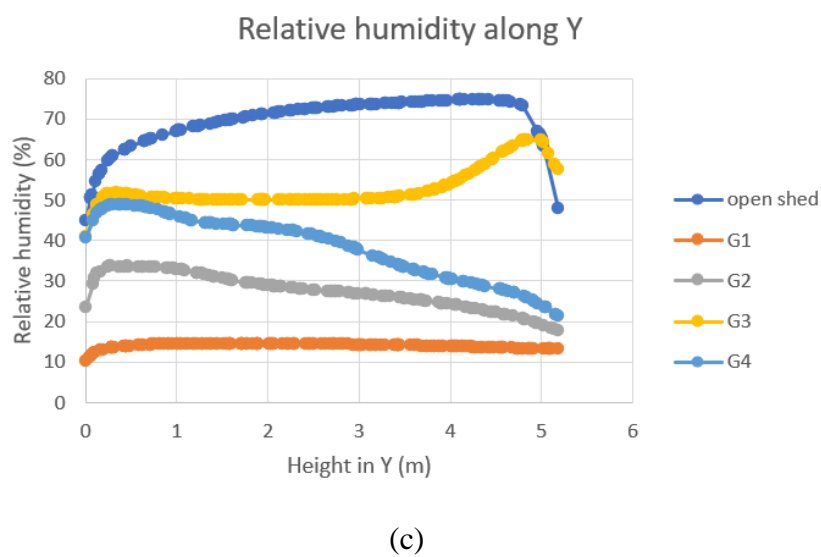
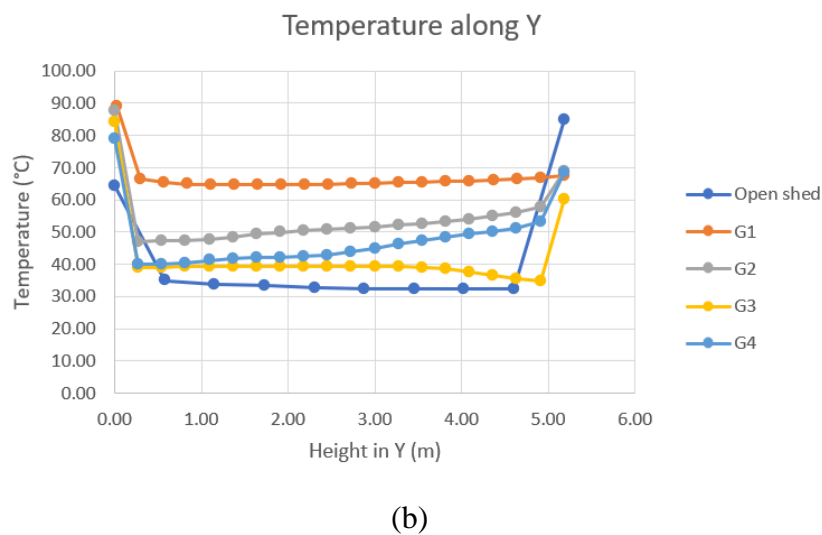
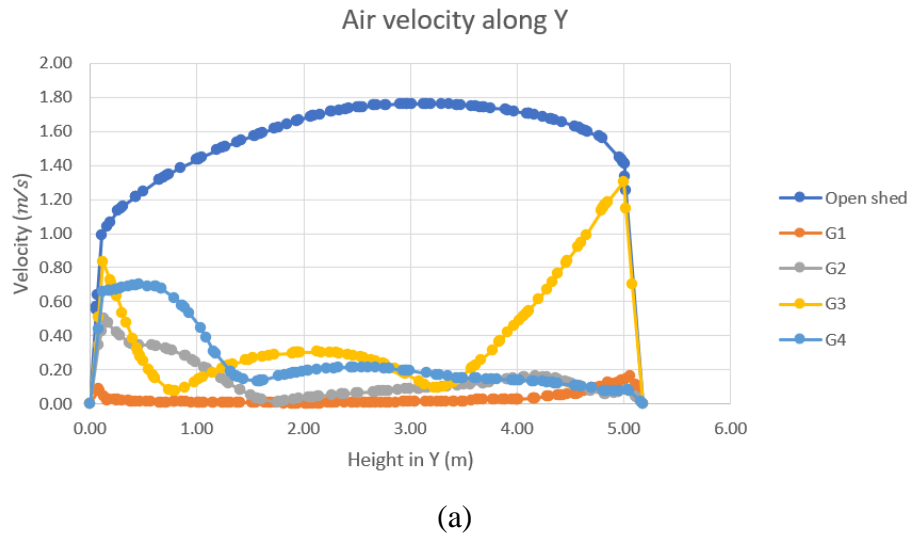


Figure 4.15: Graphs of (a) Air velocity, (b) Temperature and (c) RH along the height in Y

From the velocity magnitude contour of G4 (Figure 4.13(a)), it can be observed that the air flowing into the dryer through the opening on east side and moves downward to the bottom region near the floor. The air is then flowing out the dryer through the exhaust fan on the west side. A poor air flow was observed at the upper east region of G4. The air flow pattern in G4 was found similar to G2. However, the air flow in G4 was found better than G2 as it can be observed in Figure 4.15(a) that the air velocity along the height in G4 is higher than G2. Besides, an air circulation was observed in the lower middle region of G4. Air circulation could provide a better air mixing in the region. The computed mass flow rate at the exhaust fan was 1.52 kg/s which was higher than G2 but lower than G3.

The temperature distribution in G4 can be observed in Figure 4.14(a). It can be observed that lower temperatures were found near the opening on the east side where the ambient air flowing in. The regions with relatively higher temperature were coincided with the regions having low air movement. The RH distribution in G4 was found as expected (Figure 4.14(b)), the distribution of RH was inverse to the temperatures where the lower RH values were found in higher temperature regions.

The computed average temperature and RH in G4 were 44.2 °C and 40 %. The average mass flow rate, temperature and RH in G4 were in between G2 and G3. Therefore, G4 has an optimum drying environment compared to G2 and G3 due to the compromise between heat retention and ventilation performance. By comparing to open-shed dryer, G4 was able to provide 11.2 °C higher temperature. Besides, G4 was able to obtain 29.8 % lower RH than open-shed dryer. The improvement in drying rate achieved by G4 was predicted based on the study by Chandramohan (2018) in drying a rectangular shaped moist sample in a similar temperature range. It was found that G4 was able improve the drying rate by 52.4 % compared to open-shed dryer.

There are several studies on the drying environment of GHSDs by other researchers were reviewed in this study. Almuhanha (2012) constructed a gable-even span GHSD covered by fiberglass sheets and with an exhaust fan installed. The dimensions of the GHSD were 2 m (L) × 1 m (w) × 1.2 m (H) and it was located in Saudi Arabia. The GHSD provided an increment of air temperature by 14.1 °C. Thus, G4 has a 1 °C lower increment of air temperature than the

GHSD by Almuhanha. The average temperature in the GHSD was 47.7 °C which is 3.5 °C higher than the average temperature in G4.

Jitjack et al. (2016) constructed a parabolic shaped GHSD in Thailand. The GHSD was covered by polycarbonate sheets and with an exhaust fan installed. The dimensions of the GHSD were 3.5 m (L) × 2 m (w) × 1.5 m (H). The GHSD was able to increase the air temperature by 14.3 °C which is 1.2 °C higher than the increment of air temperature provided by G4. The average temperature in the GHSD by Jitjack was 44.3 °C which is similar to the average temperature (44.2 °C) in G4.

#### 4.8 Orientation of paperboard samples in the dryer

Besides of the discussed factors including air flow, temperature and RH, the orientation of the drying samples in the dryer could be a minor factor in affecting the drying rate. The drying sample in this study was the paperboard. There were two different orientations (Figure 4.16) studied by implementing steady state CFD simulation with the same meshing, procedure and solution method. There were two paperboard samples with the dimensions of 2 m × 4 m. The thickness of the paperboard samples was 2 mm. The distance between the samples was 0.6 m. However, the drying characteristic of the paperboard was not included in this study. Therefore, only the effect of orientation of samples on the air flow distribution was discussed in this study by evaluating the results of air flow vector (Figure 4.17).

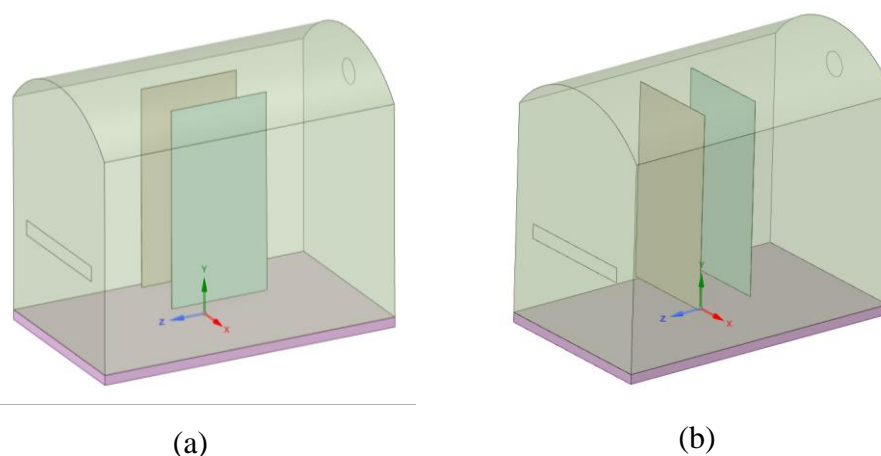
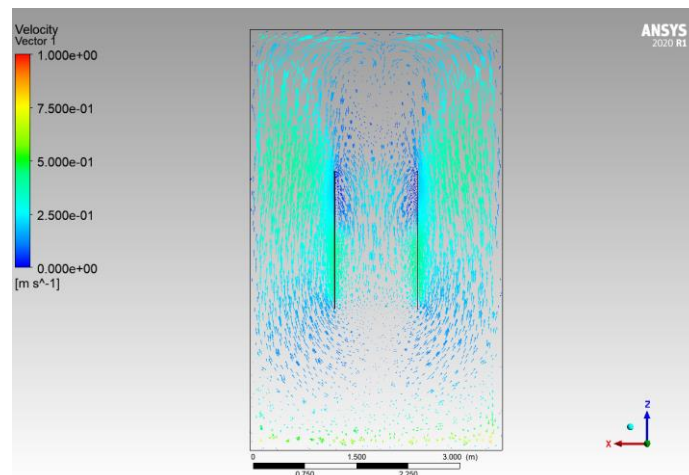
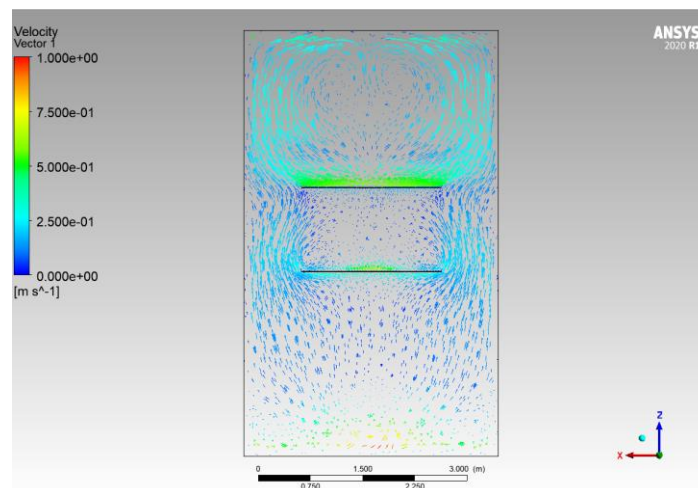


Figure 4.16: Orientations of paperboard samples in (a) Parallel and (b) Normal to inflow of air.



(a)



(b)

Figure 4.17: Velocity vector around the paperboard samples oriented in (a) Parallel and (b) Normal to the inflow of air

From the Figure 4.17, it can be observed that the air movement between the samples was better when the samples are oriented in parallel to the air flowing into the dryer. The air movement between the samples in normal oriented was poor due to the air blockage by the sample near the inlet opening. Hence, the sample further away from the inlet opening received a minimum air flow. The poor air movement in the region between the samples could result in the accumulation of moisture during the drying process. The accumulated moisture around the surfaces of paperboard samples could slow down the drying of the particular surfaces and thus causing an ununiform drying. Therefore, the paperboard samples are recommended to be oriented in parallel to the inflowing air to achieve a better drying.

#### **4.9 Summary**

The results of the air flow, temperature and RH distributions in the open-shed dryer and GHSDs were analysed to compare the drying performance between open-shed and GHSD. It was found that GHSD has better drying performance than open-shed dryer by providing a more favourable drying environment with controlled air flow, increased temperature and decreased RH in the dryer. Besides the results have also shown the effect of openings configurations on the drying environment in GHSD. The arrangement and size of openings could affect the ventilation performance of the GHSD in terms of mass flow rate. A higher mass flow rate could improve the air movement in the GHSD. However, an optimum mass flow rate is required to ensure the heat retention in the GHSD. Based on the evaluated results, an optimized GHSD, G4 was proposed. The idea of the design of G4 was to achieve a compromise between ventilation and heat retention performance. The results have shown that the drying environment in G4 was able to achieve 11.2 °C higher temperature and 29.8 % lower RH which led to an improvement of drying rate by 52.4 % compared to open-shed dryer. Lastly, the orientation of the paperboard samples was suggested in parallel to the inflow to achieve better drying.

## CHAPTER 5

### CONCLUSION AND RECOMMENDATIONS

#### 5.1 Conclusion

In this study, the drying performance of open-shed dryer and GHSD was compared and discussed by evaluating the drying environment in the dryers. CFD simulation was implemented in this study to determine the distribution of air flow, temperature and RH in the dryers that have a great influence on the drying rate of the paperboard. The models of an open-shed dryer and three GHSDs with different openings configurations were constructed to perform the CFD simulation. The results including the contour plots and graphs have shown that GHSD is able to provide a better drying performance compared to open-shed dryer by providing a drying environment with controlled air flow, higher temperature and lower RH. It was found that GHSD is able provide an increment of temperature in the range of 6.7 to 32.6 °C and a decrement of RH in the range of 19.6 to 55.7 %.

The drying performance of GHSD models with different openings configurations (G1, G2 and G3) were analyzed in CFD simulation results. It was found that the arrangement and size of the openings have a great impact on the distribution of air flow, temperature and RH in the GHSD. The larger area of openings has higher mass flow rate across which was found able to increase the air movement in the GHSD. The mass flow rate indicated the ventilation performance of the GHSD. However, the high mass flow rate could cause excessive air exchange between the internal and external environment of the GHSD which could results in poor heat retention.

Based on the evaluated results, a GHSD, G4 with optimized design was proposed. The idea adopted on the modification and optimization of the design was based on obtaining a compromise between the ventilation and heat retention performance by implementing mechanical ventilation with natural ventilation. An exhaust fan with 0.5 m diameter and 7240 m<sup>3</sup>/h air flow rate was implemented on the west side of the dryer. An opening with an area of 0.78 m<sup>2</sup> was located on the east side of the dryer. The geometry, cover material and floor material were same as the evaluated GHSDs. The results showed that an



optimum air movement which provides a better air mixing was found in G4 compared to G2 and G3. The average temperature and RH obtained in G4 was 11.2 °C higher and 29.8 % lower respectively than the open-shed dryer. It was found that the drying rate achieved by G4 was 52.4 % better than the open-shed dryer.

The orientation of the paperboard samples in the dryer during the drying process was studied by focusing on the influence of the orientation of paperboard samples on the air flow patterns in the dryer. The paperboard samples were oriented in parallel and normal to the inflow of air. The air flow around the samples was visualized in velocity vectors. A poor air flow was found in the region between the samples, when they were oriented in normal to the inflow of air. On the other hand, orientation in parallel to the inflow of air was recommended as it allows the samples expose to a more uniform air flow. An uniform air flow across the surface of the paperboard samples could avoid the accumulation of moisture around the surface slowing down the drying process.

## **5.2 Recommendations for future work**

In the current study, steady state CFD simulations were performed to study the internal climate of the open-shed dryer and GHSDs without considering the changes of air flow, temperature and RH over time. In order to study the changes in the internal climate of the dryers according to the variation of external environment hourly, transient simulation is recommended as it is able to show the evolution of flow over time. Furthermore, grid independence check is recommended in future studies to ensure an optimum mesh size for the models in order to obtain solution with satisfied quality and lowest possible computational cost.

Although CFD simulation was found to be a reliable tool to predict the drying performance of the dryers, an actual experimental work is recommended to be carried out in the future studies to determine the validity of the CFD models. Besides, the drying rate of the paperboard samples can be obtained from the experimental work to allow a more realistic prediction for the drying performance of the dryers.

The conducted study on GHSD in this current work focused on the effect of openings configurations on the distribution of air flow, temperature and RH in the dryers. It has been shown that the size of the opening on the dryer plays an important role in controlling the drying environment. Therefore, one of the objectives in the future studies can be focused on determining the optimum area of opening with respect to the floor area in the GHSD.

## REFERENCES

Afou, Y. EL, Msaad, A.A., Kousksou, T. and Mahdaoui, M., 2015. Predictive control of temperature under greenhouse using LQG strategy. In: *Proceedings of 2015 IEEE International Renewable and Sustainable Energy Conference, IRSEC 2015*. IEEE.

Agrawal, A. and Sarviya, R.M., 2016. A review of research and development work on solar dryers with heat storage. *International Journal of Sustainable Energy*, 35(6), pp.583–605.

Ahmad, A. and Prakash, O., 2020. Performance evaluation of a solar greenhouse dryer at different bed conditions under passive mode. *Journal of Solar Energy Engineering, Transactions of the ASME*, 142(1), pp.1–10.

Al-Hilphy, A.R., Gavahian, M., Barba, F.J., Lorenzo, J.M., Al-Shalah, Z.M. and Verma, D.K., 2020. Drying of sliced tomato (*Lycopersicon esculentum* L.) by a novel halogen dryer: Effects of drying temperature on physical properties, drying kinetics, and energy consumption. *Journal of Food Process Engineering*, 44(3).

Almuhanna, E.A., 2012. Utilization of a Solar Greenhouse as a Solar Dryer for Drying Dates under the Climatic Conditions of the Eastern Province of Saudi Arabia. *Journal of Agricultural Science*, 4(3), pp.237–246.

Ansys Fluent, 2013. MAN - ANSYS Fluent User' s Guide Release 15.0. *Knowledge Creation Diffusion Utilization*, 15317(November), pp.724–746.

Ayyappan, S., Mayilsamy, K. and Sreenarayanan, V. V., 2016. Performance improvement studies in a solar greenhouse drier using sensible heat storage materials. *Heat and Mass Transfer/Waerme- und Stoffuebertragung*, [online] 52(3), pp.459–467. Available at: <<http://dx.doi.org/10.1007/s00231-015-1568-5>>.

Azaizia, Z., Kooli, S., Hamdi, I., Elkhail, W. and Guizani, A.A., 2020. Experimental study of a new mixed mode solar greenhouse drying system with and without thermal energy storage for pepper. *Renewable Energy*, [online] 145, pp.1972–1984. Available at: <<https://doi.org/10.1016/j.renene.2019.07.055>>.

Badaoui, O., Hanini, S., Djebli, A., Haddad, B. and Benhamou, A., 2019. Experimental and modelling study of tomato pomace waste drying in a new solar greenhouse: Evaluation of new drying models. *Renewable Energy*, [online] 133, pp.144–155. Available at: <<https://doi.org/10.1016/j.renene.2018.10.020>>.

Bañuelos-Ruedas, F., Angeles-Camacho, C. and Rios-Marcuello, S., 2010. Analysis and validation of the methodology used in the extrapolation of wind speed data at different heights. *Renewable and Sustainable Energy Reviews*, 14(8), pp.2383–2391.

Berroug, F., Lakhali, E.K., El Omari, M., Faraji, M. and El Qarnia, H., 2011. Thermal performance of a greenhouse with a phase change material north wall. *Energy and Buildings*, [online] 43(11), pp.3027–3035. Available at: <<http://dx.doi.org/10.1016/j.enbuild.2011.07.020>>.

Bhaskara Rao, T.S.S. and Murugan, S., 2021. Solar drying of medicinal herbs: A review. *Solar Energy*, [online] 223(October 2020), pp.415–436. Available at: <<https://doi.org/10.1016/j.solener.2021.05.065>>.

Boulard, T., Razafinjohany, E., Baille, A., Jaffrin, A. and Fabre, B., 1990. Performance of a greenhouse heating system with a phase change material. *Agricultural and Forest Meteorology*, 52(3–4), pp.303–318.

Boulard, T. and Wang, S., 2002. Experimental and numerical studies on the heterogeneity of crop transpiration in a plastic tunnel. *Computers and Electronics in Agriculture*, 34(1–3), pp.173–190.

Caparanga, A.R., Reyes, R.A.L., Rivas, R.L., De Vera, F.C., Retnasamy, V. and Aris, H., 2017. Effects of air temperature and velocity on the drying kinetics and product particle size of starch from arrowroot (*Maranta arundinacea*). *EPJ Web of Conferences*, 162, pp.4–8.

Chandramohan, V.P., 2018. Influence of air flow velocity and temperature on drying parameters: An experimental analysis with drying correlations. *IOP Conference Series: Materials Science and Engineering*, 377(1).

Chanpet, M., Rakmak, N., Matan, N. and Siripatana, C., 2020. Effect of air velocity, temperature, and relative humidity on drying kinetics of rubberwood. *Heliyon*, [online] 6(10), p.e05151. Available at: <<https://doi.org/10.1016/j.heliyon.2020.e05151>>.

Chayjan, R.A., Alizade, H.H.A. and Shadidi, B., 2012. Modeling of some pistachio drying characteristics in fix, semi fluid and fluid bed dryer. *Agricultural Engineering International: CIGR Journal*, 14(2), pp.143–154.

Chinenye, N.M., 2009. Effect of Drying Temperature and Drying Air Velocity on the Drying Rate and Drying Constant of Cocoa Bean. *Agricultural Engineering International: CIGR Journal*, 11(1), pp.1–7.

Condorí, M. and Saravia, L., 1998. The performance of forced convection greenhouse driers. *Renewable Energy*, 13(4), pp.453–469.

Doymaz, I., 2005. Thin-layer drying behaviour of mint leaves. *Journal of Food Engineering*, 74(3), pp.370–375.

Dragičević, S.M., 2011. Determining the optimum orientation of a greenhouse on the basis of the total solar radiation availability. *Thermal Science*, 15(1), pp.215–221.

Duong, Y.H.P., Vo, N.T., Le, P.T.K. and Tran, V.T., 2021. Three-dimensional simulation of solar greenhouse dryer. *Chemical Engineering Transactions*, 83, pp.211–216.

ELkhadraoui, A., Kooli, S., Hamdi, I. and Farhat, A., 2015. Experimental investigation and economic evaluation of a new mixed-mode solar greenhouse dryer for drying of red pepper and grape. *Renewable Energy*, [online] 77, pp.1–8. Available at: <<http://dx.doi.org/10.1016/j.renene.2014.11.090>>.

Flores-Velazquez, J., Montero, J.I., Baeza, E.J. and Lopez, J.C., 2014. Mechanical and natural ventilation systems in a greenhouse designed using computational fluid dynamics. *International Journal of Agricultural and Biological Engineering*, 7(1), pp.1–16.

Forest Products Laboratory, 1999. Air Drying of Lumber. *Methods*, p.62.

Ghosh, A.K., 2011. Fundamentals of Paper Drying – Theory and Application from Industrial Perspective. *Evaporation, Condensation and Heat transfer*.

Gupta, M.J. and Chandra, P., 2002. Effect of greenhouse design parameters on conservation of energy for greenhouse environmental control. *Energy*, 27(8), pp.777–794.

El Hage, H., Herez, A., Ramadan, M., Bazzi, H. and Khaled, M., 2018. An investigation on solar drying: A review with economic and environmental assessment. *Energy*, [online] 157, pp.815–829. Available at: <<https://doi.org/10.1016/j.energy.2018.05.197>>.

Ham, C.-H., Youn, H.J. and Lee, H.L., 2020. Influence of fiber composition and drying conditions on the bending stiffness of paper. *BioResources*, 15(4), pp.9197–9211.

Hashemi, S. and Taghinezhad, E., 2011. Effects of Low Final Moisture and Drying Air Temperature on the Quality Maintenance and Breakage of Tarom Aromatic Rice ... (May).

He, X., Wang, J., Guo, S., Zhang, J., Wei, B., Sun, J. and Shu, S., 2018. Ventilation optimization of solar greenhouse with removable back walls based on CFD. *Computers and Electronics in Agriculture*, [online] 149(March 2017), pp.16–25. Available at: <<https://doi.org/10.1016/j.compag.2017.10.001>>.

Inyang, U.E., Oboh, I.O. and Etuk, B.R., 2018. Kinetic Models for Drying Techniques—Food Materials. *Advances in Chemical Engineering and Science*, 08(02), pp.27–48.

Jain, D. and Tiwari, G.N., 2004. Effect of greenhouse on crop drying under natural and forced convection I: Evaluation of convective mass transfer coefficient. *Energy Conversion and Management*, 45(5), pp.765–783.

Jamaledine, T.J. and Ray, M.B., 2010. Application of computational fluid dynamics for simulation of drying processes: A review. *Drying Technology*, 28(2), pp.120–154.

Janjai, S., 2012. A greenhouse type solar dryer for small-scale dried food industries: Development and dissemination. *International Journal Of Energy and Environment*, [online] 3(3), pp.383–398. Available at: <[http://ijee.ieefoundation.org/vol2/public\\_html/ijeeindex/vol2/issue4/IJEE\\_03\\_v2n4.pdf](http://ijee.ieefoundation.org/vol2/public_html/ijeeindex/vol2/issue4/IJEE_03_v2n4.pdf)>.

Jitjack, K., Thepa, S., Sudaprasert, K. and Namprakai, P., 2016. Improvement of a rubber drying greenhouse with a parabolic cover and enhanced panels. *Energy and Buildings*, [online] 124, pp.178–193. Available at: <<http://dx.doi.org/10.1016/j.enbuild.2016.04.030>>.

Kamarulzaman, A., Hasanuzzaman, M. and Rahim, N.A., 2021. Global advancement of solar drying technologies and its future prospects: A review. *Solar Energy*, [online] 221(December 2020), pp.559–582. Available at: <<https://doi.org/10.1016/j.solener.2021.04.056>>.

Khanlari, A., Sözen, A., Şirin, C., Tuncer, A.D. and Gungor, A., 2020. Performance enhancement of a greenhouse dryer: Analysis of a cost-effective alternative solar air heater. *Journal of Cleaner Production*, 251.

Kim, K., Yoon, J.Y., Kwon, H.J., Han, J.H., Eek Son, J., Nam, S.W., Giacomelli, G.A. and Lee, I.B., 2008. 3-D CFD analysis of relative humidity distribution in greenhouse with a fog cooling system and refrigerative dehumidifiers. *Biosystems Engineering*, 100(2), pp.245–255.

Kumar, M., Sansaniwal, S.K. and Khatak, P., 2016. Progress in solar dryers for drying various commodities. *Renewable and Sustainable Energy Reviews*, [online] 55, pp.346–360. Available at: <<http://dx.doi.org/10.1016/j.rser.2015.10.158>>.

Lawrence, M.G., 2005. The relationship between relative humidity and the dewpoint temperature in moist air: A simple conversion and applications. *Bulletin of the American Meteorological Society*, 86(2), pp.225–233.

Li, H., Li, Y., Yue, X., Liu, X., Tian, S. and Li, T., 2020. Evaluation of airflow pattern and thermal behavior of the arched greenhouses with designed roof ventilation scenarios using CFD simulation. *PLoS ONE*, 15(9 September), pp.1–24.

Lingayat, A., Balijepalli, R. and Chandramohan, V.P., 2021. Applications of solar energy based drying technologies in various industries – A review. *Solar Energy*, (March).

Lv, Y., Chen, L. and Chen, Q., 2010. Research on drying process of honeycomb paperboard. *2010 International Conference on Measuring Technology and Mechatronics Automation, ICMTMA 2010*, 3, pp.57–60.

Mariem, S. Ben and Mabrouk, S. Ben, 2014. Drying Characteristics of Tomato Slices and Mathematical Modeling. *International Journal of Energy Engineering* 2014, 4(2A), pp.17–24.

Mathioulakis, E., Karathanos, V.T. and Belessiotis, V.G., 1998. Simulation of air movement in a dryer by computational fluid dynamics: Application for the drying of fruits. *Journal of Food Engineering*, 36(2), pp.183–200.

Mellalou, A., Riad, W., Hnawi, S.K., Tchenka, A., Bacaoui, A. and Outzourhit, A., 2021. Experimental and CFD Investigation of a Modified Uneven-Span Greenhouse Solar Dryer in No-Load Conditions under Natural Convection Mode. *International Journal of Photoenergy*, 2021, pp.1–12.

Mesmoudi, K., Meguellati, K. and Bournet, P.E., 2017. Thermal analysis of greenhouses installed under semi arid climate. *International Journal of Heat and Technology*, 35(3), pp.474–486.

Mobtaker, H.G., Ajabshirchi, Y., Ranjbar, S.F. and Matloobi, M., 2019. Simulation of thermal performance of solar greenhouse in north-west of Iran: An experimental validation. *Renewable Energy*, [online] 135, pp.88–97. Available at: <<https://doi.org/10.1016/j.renene.2018.10.003>>.

Mohammad, S.R. and Perera, C.O., 2007. Handbook of Food Preservation second edition. *CRC Press*, pp.1–1068.

Mondal, S., Agarwala, P., Dutta, S., Naik-Nimbalkar, V., Pande, P. and Dhumal, S., 2019. Cellulosic fibre drying: fundamental understanding and process modeling. (September).

Mustayen, A.G.M.B., Mekhilef, S. and Saidur, R., 2014. Performance study of different solar dryers: A review. *Renewable and Sustainable Energy Reviews*, [online] 34, pp.463–470. Available at: <<http://dx.doi.org/10.1016/j.rser.2014.03.020>>.

Naamandadin, N.A., Sopian, A.R. and Noor, S.N.A.M., 2016. Site planning and orientation for energy efficiency: A comparative analysis on three office buildings in Kuala Lumpur to determine a location for building shading device. *Key Engineering Materials*, 700(October), pp.247–255.

Natarajan, K., Thokchom, S.S., Verma, T.N. and Nashine, P., 2017. Convective solar drying of *Vitis vinifera* & *Momordica charantia* using thermal storage materials. *Renewable Energy*, [online] 113, pp.1193–1200. Available at: <<http://dx.doi.org/10.1016/j.renene.2017.06.096>>.

Norton, T., Sun, D.W., Grant, J., Fallon, R. and Dodd, V., 2007. Applications of computational fluid dynamics (CFD) in the modelling and design of ventilation systems in the agricultural industry: A review. *Bioresource Technology*, 98(12), pp.2386–2414.

Odhiambo, O., 2016. Development of Improved Orange Flesh Sweet Potato Dryers in Western Kenya. *Technical Report*, (November), pp.1–26.

- Patil, R. and Gawande, R., 2016. A review on solar tunnel greenhouse drying system. *Renewable and Sustainable Energy Reviews*, 56, pp.196–214.
- Piscia, D., Montero, J.I., Baeza, E. and Bailey, B.J., 2012. A CFD greenhouse night-time condensation model. *Biosystems Engineering*, [online] 111(2), pp.141–154. Available at: <<http://dx.doi.org/10.1016/j.biosystemseng.2011.11.006>>.
- Ramírez, C., Astorga, V., Nuñez, H., Jaques, A. and Simpson, R., 2017. Anomalous diffusion based on fractional calculus approach applied to drying analysis of apple slices: The effects of relative humidity and temperature. *Journal of Food Process Engineering*, 40(5), pp.1–10.
- Román-Roldán, N.I., López-Ortiz, A., Ituna-Yudonago, J.F., García-Valladares, O. and Pilatowsky-Figueroa, I., 2019. Computational fluid dynamics analysis of heat transfer in a greenhouse solar dryer “chapel-type” coupled to an air solar heating system. *Energy Science and Engineering*, 7(4), pp.1123–1139.
- Sahdev, R.K., Kumar, M. and Dhingra, A.K., 2016. A review on applications of greenhouse drying and its performance. *Agricultural Engineering International: CIGR Journal*, 18(2), pp.395–412.
- Sasongko, S.B., Hadiyanto, H., Djaeni, M., Perdanianti, A.M. and Utari, F.D., 2020. Effects of drying temperature and relative humidity on the quality of dried onion slice. *Heliyon*, [online] 6(7), p.e04338. Available at: <<https://doi.org/10.1016/j.heliyon.2020.e04338>>.
- Senhaji, A., Mouqallid, M. and Majdoubi, H., 2019. CFD Assisted Study of Multi-Chapels Greenhouse Vents Openings Effect on Inside Airflow Circulation and Microclimate Patterns. *Open Journal of Fluid Dynamics*, 09(02), pp.119–139.
- Sethi, V.P., 2009. On the selection of shape and orientation of a greenhouse: Thermal modeling and experimental validation. *Solar Energy*, [online] 83(1), pp.21–38. Available at: <<http://dx.doi.org/10.1016/j.solener.2008.05.018>>.
- Sharma, A., Chen, C.R. and Vu Lan, N., 2009. Solar-energy drying systems: A review. *Renewable and Sustainable Energy Reviews*, 13(6–7), pp.1185–1210.
- Srinivasan, G. and Muthukumar, P., 2021. A review on solar greenhouse dryer: Design, thermal modelling, energy, economic and environmental aspects. *Solar Energy*, [online] (October 2020). Available at: <<https://doi.org/10.1016/j.solener.2021.04.058>>.
- Swarno, H.A., Zaki, S.A., Hagishima, A. and Yusup, Y., 2020. Characteristics of wind speed during rainfall event in the tropical urban city. *Urban Climate*, 32(January).



Tham, T.C., Ng, M.X., Gan, S.H., Chua, L.S., Aziz, R., Chuah, L.A., Hii, C.L., Ong, S.P., Chin, N.L. and Law, C.L., 2017. Effect of ambient conditions on drying of herbs in solar greenhouse dryer with integrated heat pump. *Drying Technology*, 35(14), pp.1721–1732.

Thirugnanasambandam, M., Iniyan, S. and Goic, R., 2010. A review of solar thermal technologies. *Renewable and Sustainable Energy Reviews*, 14(1), pp.312–322.

TIGAMPO, S., SAMBOU, V., DIEYE, Y., TOURE, P.M. and BODIAN, S., 2020. Study of Air Movement and Temperature Distribution in a Greenhouse Used as a Dryer. *MATEC Web of Conferences*, 330, p.01046.

Tiwari, S., Tiwari, G.N. and Al-Helal, I.M., 2016. Performance analysis of photovoltaic-thermal (PVT) mixed mode greenhouse solar dryer. *Solar Energy*, [online] 133, pp.421–428. Available at: <<http://dx.doi.org/10.1016/j.solener.2016.04.033>>.

Tomar, V., Tiwari, G.N. and Norton, B., 2017. Solar dryers for tropical food preservation: Thermophysics of crops, systems and components. *Solar Energy*, [online] 154, pp.2–13. Available at: <<http://dx.doi.org/10.1016/j.solener.2017.05.066>>.

Udomkun, P., Romuli, S., Schock, S., Mahayothee, B., Sartas, M., Wossen, T., Njukwe, E., Vanlauwe, B. and Müller, J., 2020. Review of solar dryers for agricultural products in Asia and Africa: An innovation landscape approach. *Journal of Environmental Management*, [online] 268(May), p.110730. Available at: <<https://doi.org/10.1016/j.jenvman.2020.110730>>.

Villagrán, E. and Bojacá, C., 2020. Study using a CFD approach of the efficiency of a roof ventilation closure system in a multi-tunnel greenhouse for nighttime microclimate optimization. *Revista Ceres*, 67(5), pp.345–356.

Villagran, E., Henao-Rojas, J.C. and Franco, G., 2021. Thermo-environmental performance of four different shapes of solar greenhouse dryer with free convection operating principle and no load on product. *Fluids*, 6(5).

Villagran, E., Leon, R., Rodriguez, A. and Jaramillo, J., 2020. 3D numerical analysis of the natural ventilation behavior in a Colombian greenhouse established in warm climate conditions. *Sustainability (Switzerland)*, 12(19).

Vivekanandan, M., Periasamy, K., Babu, C.D., Selvakumar, G. and Arivazhagan, R., 2021. Experimental and CFD investigation of six shapes of solar greenhouse dryer in no load conditions to identify the ideal shape of dryer. *Materials Today: Proceedings*, [online] 37(Part 2), pp.1409–1416. Available at: <<https://doi.org/10.1016/j.matpr.2020.07.062>>.

Xin, Y.N., Zhang, J.W. and Li, B., 2018. Drying kinetics of tobacco strips at different air temperatures and relative humidities. *Journal of Thermal Analysis and Calorimetry*, 132(2), pp.1347–1358.

Xu, W., Islam, M.N., Cao, X., Tian, J. and Zhu, G., 2021. Effect of relative humidity on drying characteristics of microwave assisted hot air drying and qualities of dried finger citron slices. *Lwt*, [online] 137(October 2020), p.110413. Available at: <<https://doi.org/10.1016/j.lwt.2020.110413>>.

Zhang, G., Fu, Z., Yang, M., Liu, X., Dong, Y. and Li, X., 2019. Nonlinear simulation for coupling modeling of air humidity and vent opening in Chinese solar greenhouse based on CFD. *Computers and Electronics in Agriculture*, [online] 162(January 2018), pp.337–347. Available at: <<https://doi.org/10.1016/j.compag.2019.04.024>>.

Zomorodian, A.A. and Dadashzadeh, M., 2009. Indirect and mixed mode solar drying mathematical models for sultana grape. *Journal of Agricultural Science and Technology*, 11(4), pp.391–400.

## APPENDICES

### Appendix A: UDF coding

```

#include "udf.h"
#define UREF 1.8
#define CMU 0.09
#define VKC 0.4
#define ZREF 10.0
#define Z0 0.2

DEFINE_PROFILE(velocity_profile, thread, position)
{
    float x[ND_ND];
    float y;
    float u, u_star;
    face_t f;

    u_star = UREF*VKC/log((ZREF+Z0)/Z0) ; // ref [1]

    begin_f_loop(f, thread)
    {
        F_CENTROID(x,f,thread);
        y=x[1];
        u = u_star/VKC*log((y+Z0)/Z0);
        F_PROFILE(f,thread,position) = u;
    }
    end_f_loop(f, thread)
}

/* profile for kinetic energy */

DEFINE_PROFILE(k_profile, thread, position)
{
    float x[ND_ND];
    face_t f;

    float u_star ;

    u_star = UREF*VKC/log((ZREF+Z0)/Z0) ; // ref [1]

    begin_f_loop(f, thread)
    {
        F_CENTROID(x,f,thread);

        F_PROFILE(f,thread,position)=u_star*u_star/sqrt(CMU);
    }
    end_f_loop(f, thread)
}

/* profile for dissipation rate */

DEFINE_PROFILE(dissip_profile, thread, position)
{
    float x[ND_ND];
    face_t f;
    float u_star, y ;

    u_star = UREF*VKC/log((ZREF+Z0)/Z0) ; // ref [2]

    begin_f_loop(f, thread)
    {
        F_CENTROID(x,f,thread);
        y=x[1];
        F_PROFILE(f,thread,position)=pow(u_star,3.)/(VKC*(y+Z0));
    }
    end_f_loop(f,thread)
}

```

Figure A-1: UDF coding for velocity profile

## Appendix B: Contours of air temperature

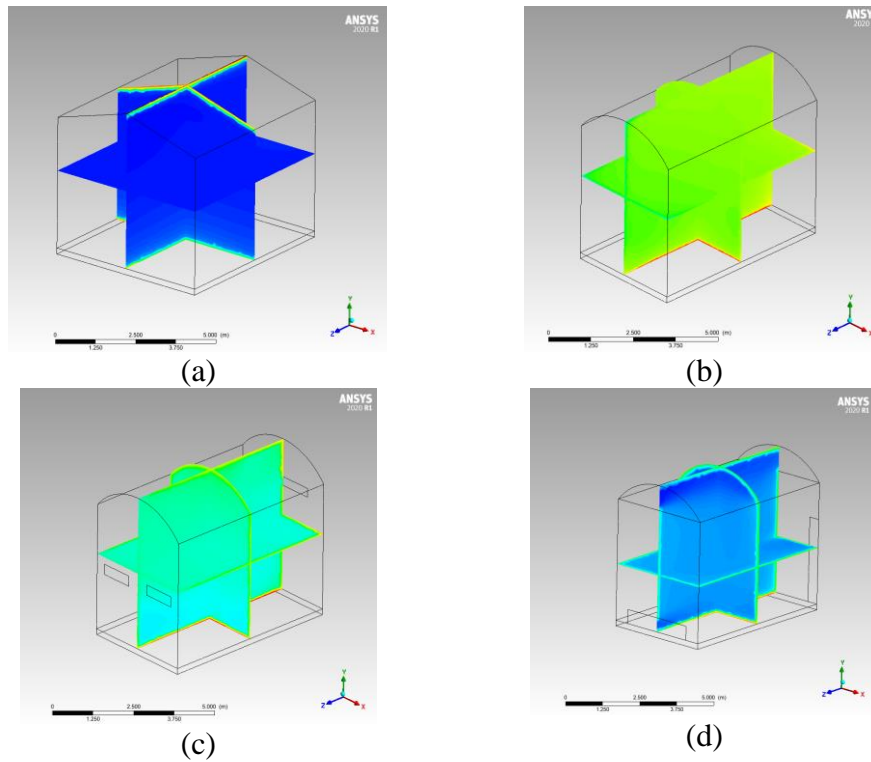


Figure B-1: Isometric view of temperature distribution in (a) Open-shed dryer, (b) G1, (c) G2 and (d) G3

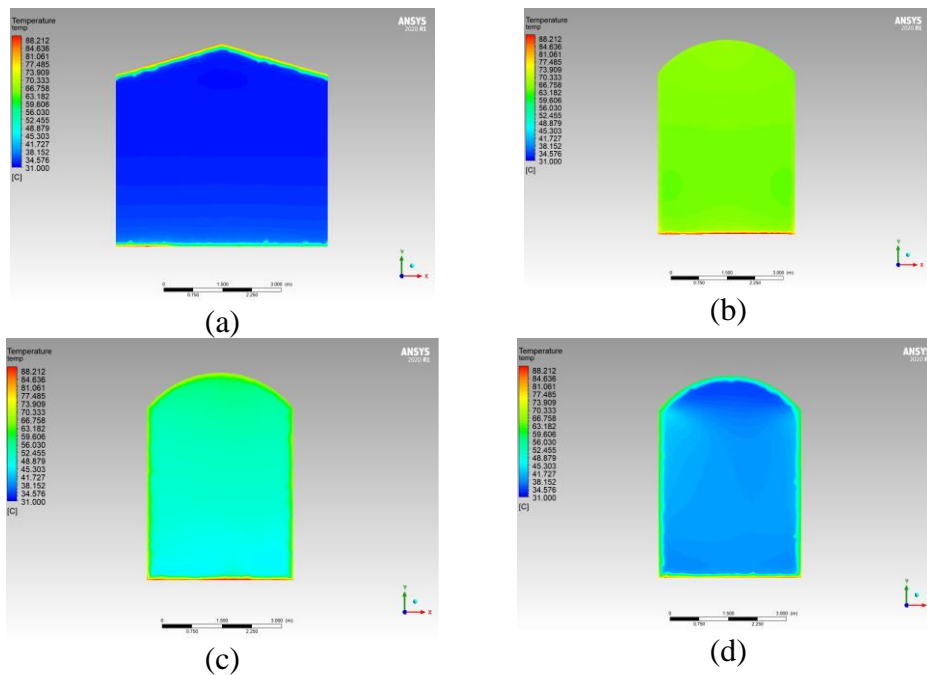


Figure B-2: Front view of temperature distribution in (a) Open-shed dryer, (b) G1, (c) G2 and (d) G3

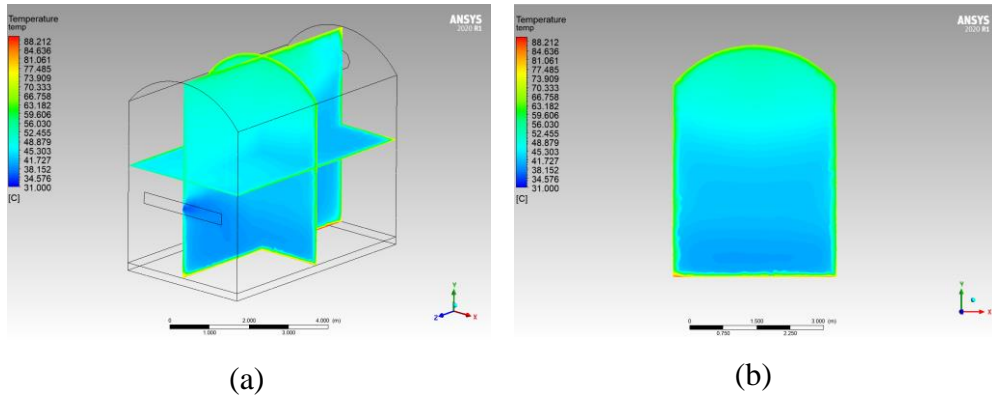


Figure B-3: (a) Isometric and (b) Front views of temperature distribution in G4

## Appendix C: Contours of RH

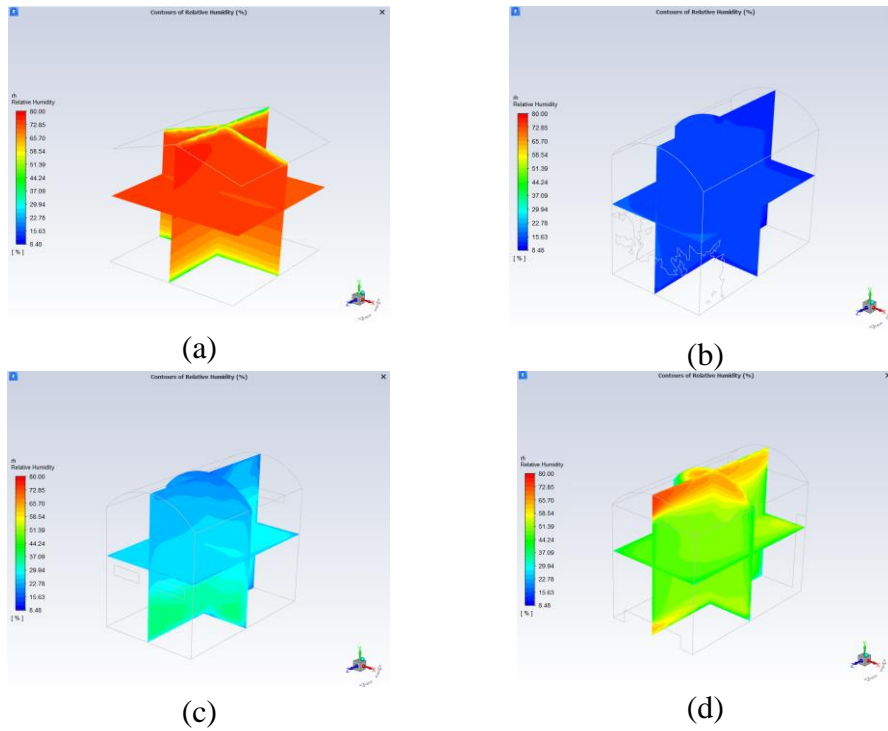


Figure C-1: Isometric view of RH distribution in (a) Open-shed dryer, (b) G1, (c) G2 and (d) G3

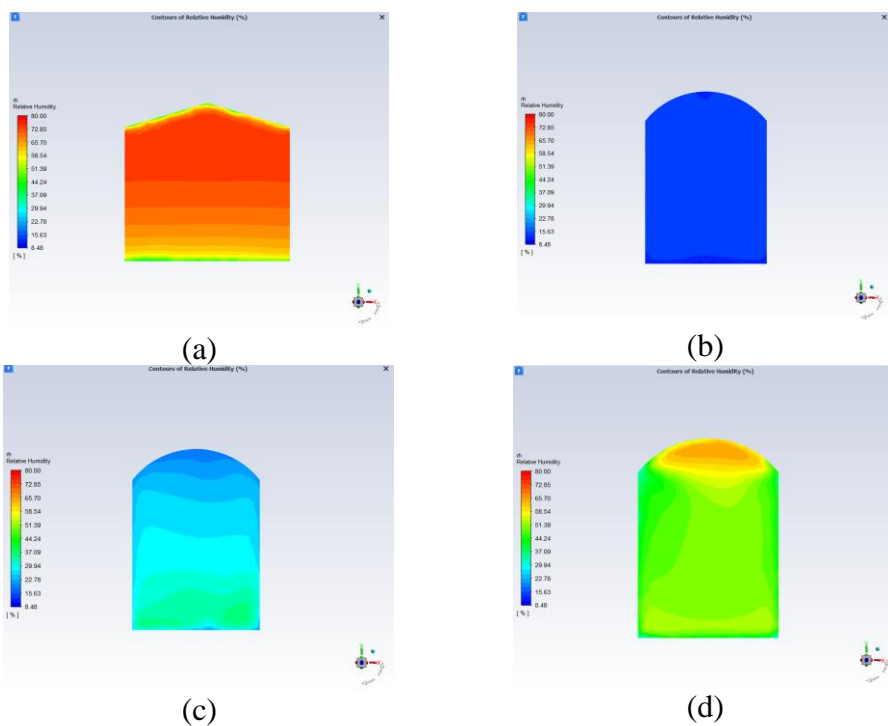


Figure C-2: Front view of RH distribution in (a) Open shed dryer, (b) G1, (c) G2 and (d) G3

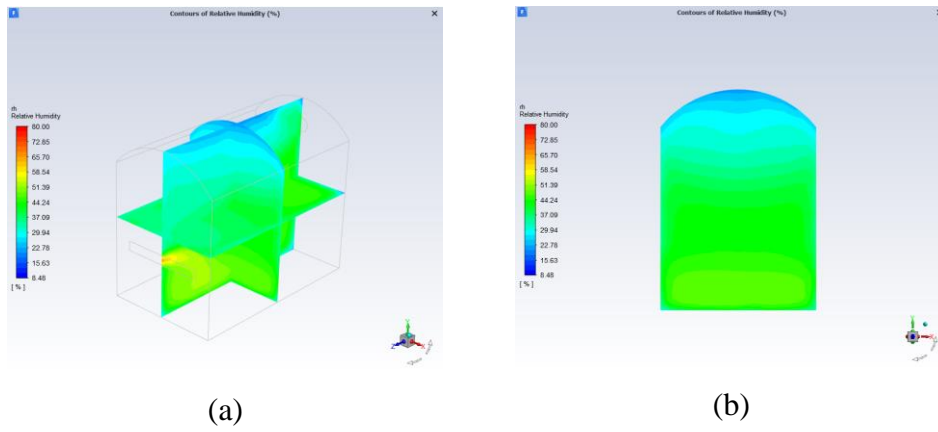


Figure C-3: (a) Isometric and (b) Front views of RH distribution in G4

## Appendix D: Contours and vectors of air velocity

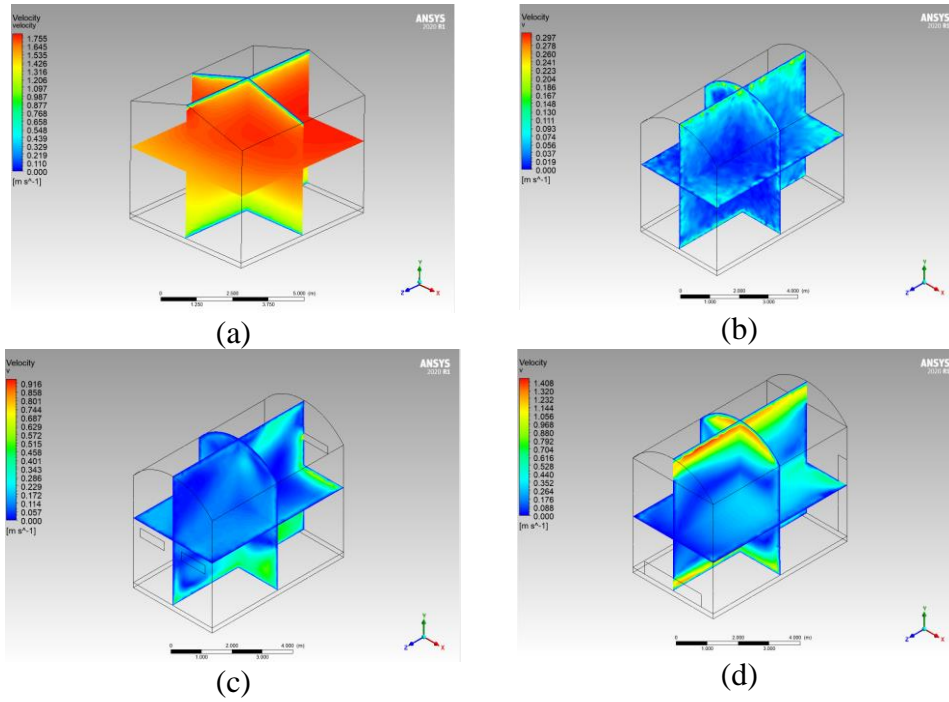


Figure D-1: Isometric view of velocity magnitude distribution in (a) Open-shed dryer, (b) G1, (c) G2 and (d) G3

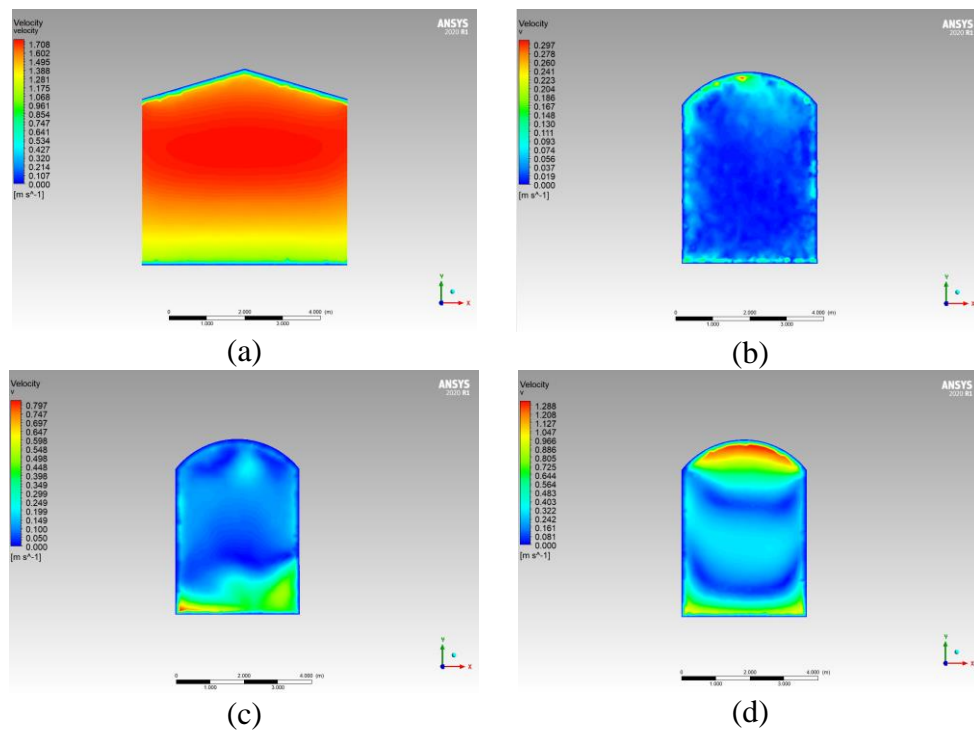


Figure D-2: Front view of velocity magnitude distribution in (a) Open-shed dryer, (b) G1, (c) G2 and (d) G3



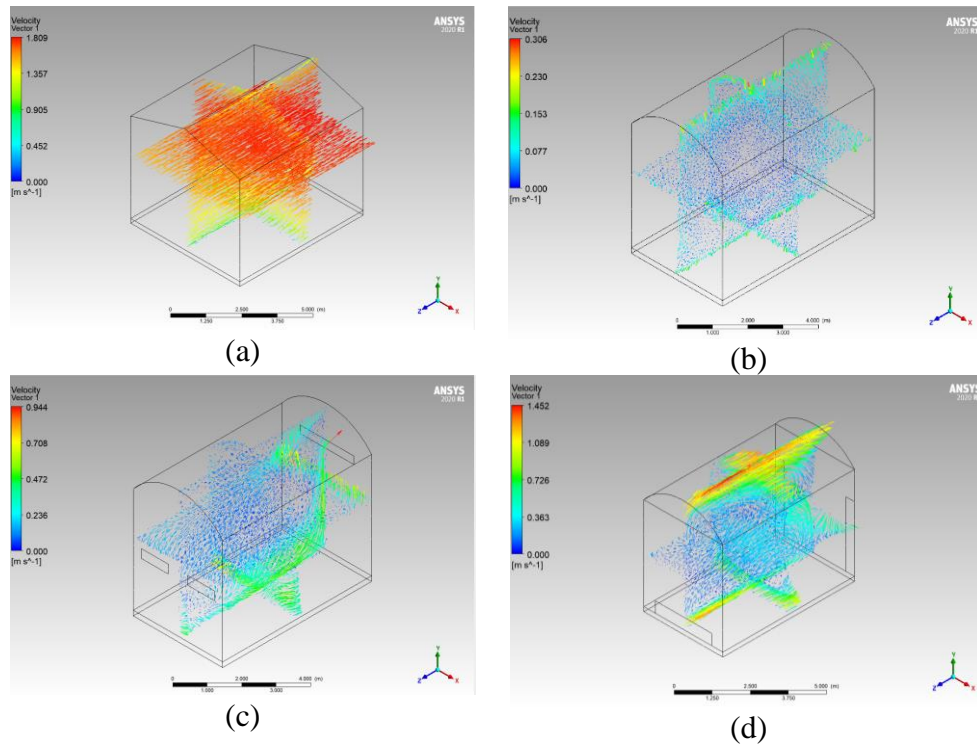


Figure D-3: Isometric view of velocity vector in (a) Open-shed dryer, (b) G1, (c) G2 and (d) G3

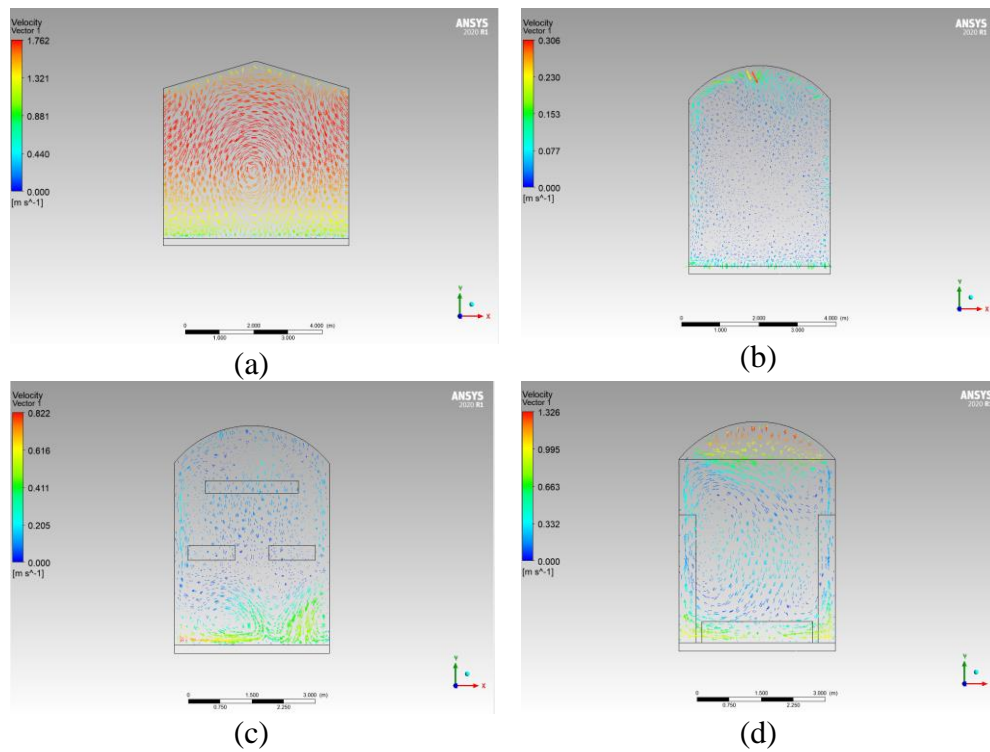


Figure D-4: Front view of velocity vector in (a) Open-shed dryer, (b) G1, (c) G2 and (d) G3

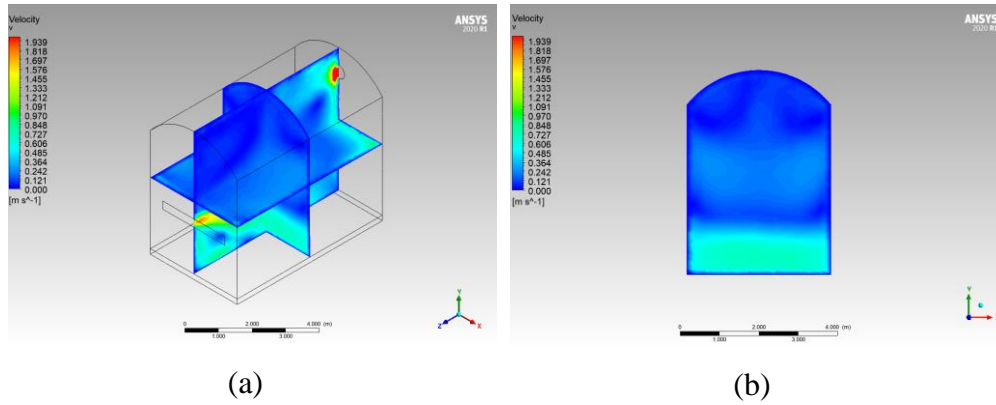


Figure D-5: (a) Isometric and (b) Front views of velocity magnitude distribution in G4

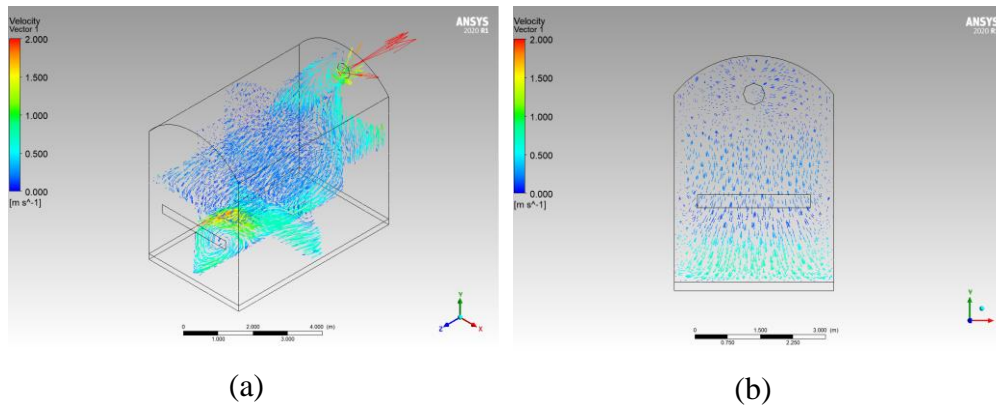
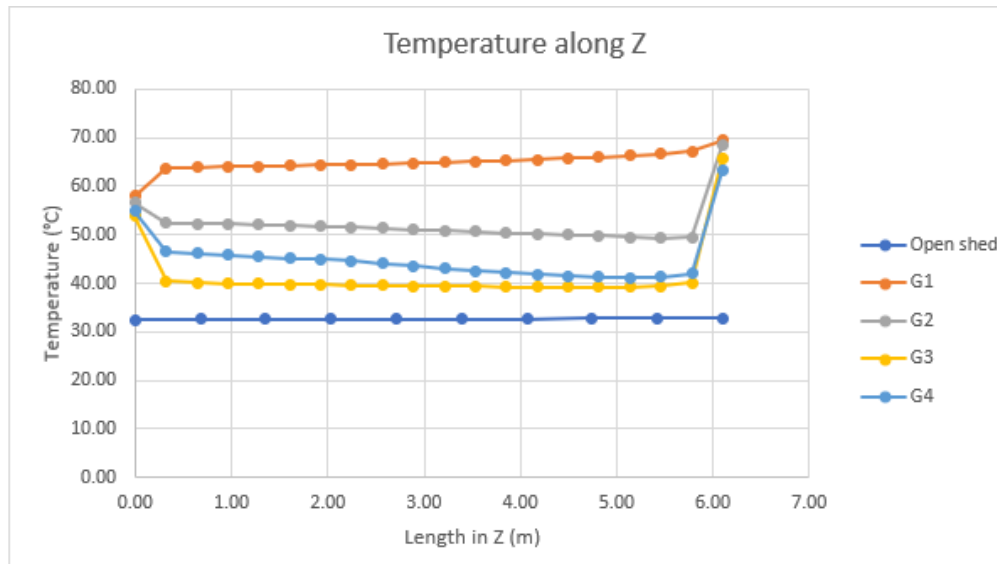
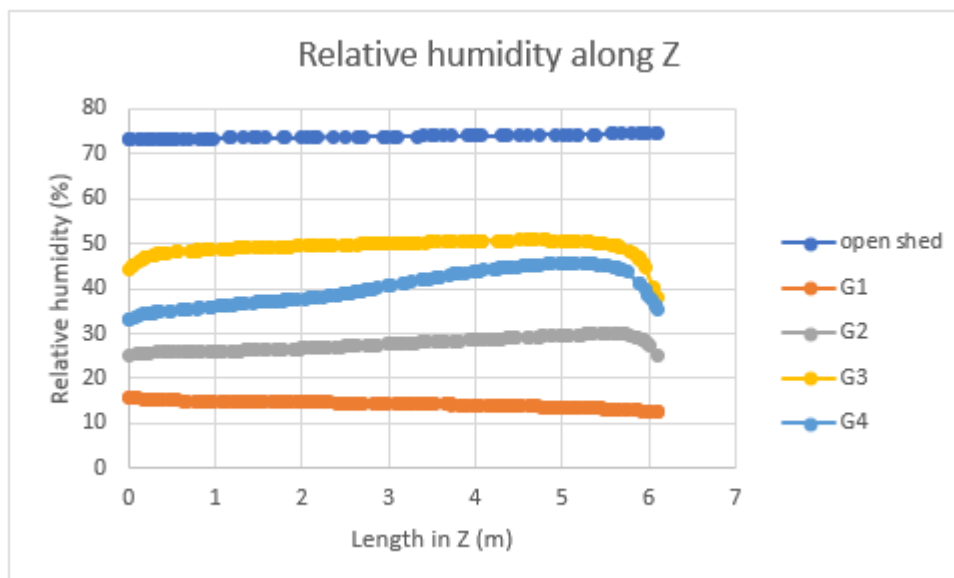


Figure D-6: (a) Isometric and (b) Front views of velocity vector in G4

## Appendix E: Graphs of temperature and RH along length in Z



(a)



(b)

Figure E-1: (a) Temperature and (b) RH along length in Z in the dryers